Hamburg University of Applied Sciences
Faculty of Life Sciences

Simulation of the cardiac electrical activity and derived body ECG using the finite element method

Master's Thesis

in the MBA program of

Biomedical Engineering

submitted by

Anna Snaidr
[redacted]

1. Examiner: Prof. Dr. Markus Riemenschneider (HAW Hamburg)
2. Examiner: Dipl.-Ing. Jürgen Sauerzapf (Personal MedSystems GmbH)

Hamburg, 01.02.2024

Abstract

Title: Simulation of the cardiac electrical activity and derived body surface ECG using the finite element method

Electrocardiography is an important tool for diagnosing and preventing heart diseases. In order to improve this technology, mathematical simulation models are employed to simulate the electrical activity within a patient's thorax and to generate an ECG on the virtual thorax surface. This is performed by the creation of heart and torso models, that represent their respective physiological characteristics mathematically. In case of the heart, complex differential equations are utilized to simulate the generation of action potentials and their propagation across the heart's tissue. To derive the corresponding ECG on the body surface, a torso geometry is modeled around the heart and assigned electrical conduction properties based on the human physiology. This allows users to place virtual electrodes on the simulated surface of the torso and analyze the resulting derived ECG.

The objective of this thesis is the development of a simulation model of the heart. This task is handled with the use of the finite element method (FEM) software COMSOL Multiphysics. In the course of this study, the model building process will be described together with the corresponding results. One of the main steps is the adjustment of the Aliev-Panfilov equations which are used to describe the electrical activity of the heart in this simulation. Subsequent steps include the integration of the geometry, the mesh generation, and the optimization of study settings.

Ultimately, the model which is generated in the course of this thesis is able to generate sufficient action potentials and accurately simulates the excitation propagation across the heart's tissue. Although there are still some improvements to be made, the model proves to be reliable and a solid foundation for future research and investigations in this field.

Keywords: electrophysiology, electrocardiogram, finite element method, cardiac modeling

Table of Content

List of Figures

List of Tables

Abbreviations and Formula Symbols

Abbreviations

Abbreviation	Description
AP	Aliev-Panfilov (model)
AV / AVN	Atrioventricular / Atrioventricular Node
BDF	Backward Differentiation Formula
CAD	Computer Aided Design
CRN	Courtemanche-Ramirez-Nattel
DICOM	Digital Imaging and Communications in Medicine
DOF	Degrees of Freedom
ECG	Electrocardiogram
Eq	Equation
FEM	Finite Element Method
FHN	FitzHugh-Nagumo (model)
HH	Hodgkin-Huxley (model)
HU	Hounsfield Unit
PDE	Partial Differential Equation
ROI	Region of interest
SA / SAN	Sinoatrial / Sinoatrial Node
TNNP	ten Tusscher-Noble-Noble-Panfilov (model)

Indices

Index	Description
act	activation value
i	integer counter variable
init	initialization value
max	maximum value
rest	resting value

Formula Symbols

Symbol	Unit	Description
C_m	F/m²	Cell Membrane Capacitance
c	S/m	Conductivity Tensor
I_{ion}	V/s	Ionic Current
σ_b	S/m	Electrical Conductivity
ε_r	As/Vm	Dielectric Constant
f	-	Source Term
∇	-	Vector of Partial Derivatives
Ω	-	Computational Domain
$\partial\Omega$	-	Domain Boundary
n	-	Outward Unit Normal Vector

1. Introduction

Cardiovascular diseases are the number one cause of death, worldwide and since decades. The number of deaths caused by these diseases increased from approximately 12 million in 1990 to 18.6 million in 2019 which emphasizes the significance of research that assesses the treatment and prevention of them. Although public health campaigns greatly contributed to raising awareness of heart diseases and the importance of a healthy lifestyle, the need for medical examinations such as electrocardiograms (ECG), ultrasound or intracardiac catheters is higher than ever. [1]

While all of these examination techniques are crucial in the process of diagnosing and treating heart diseases, only the ECG has the potential to be used in various pre-hospital settings for the purpose of preventing or at least detecting heart conditions in an early stage. Therefore, the demand for ECG devices is increasing, not only among physicians but also among patients that want to monitor their heart's health at home. The crucial difference between both application scenarios lies in the fact that devices intended for use by laymen need to be designed simple and user-friendly to ensure accurate results. One objective in the development of these ECGs is therefore the recording of a sufficient number of leads with the least number of electrodes possible. In this context, software simulating the electrophysiological behavior of the heart and the surrounding torso can be used to substantially simplify the process of developing and testing various lead-systems as well as different electrode positions.

1.1. Importance of Electrophysiological Simulations

The electrode placement on the patient's body plays a central role in the calculation of the resulting ECG and is therefore one of the major sources of error when applying an ECG. Even small inaccuracies in the positioning of electrodes can lead to significant changes in the resulting ECG and therefore a corruption of the results. To eliminate this source of error, the reduction of electrodes and the identification of robust and prominent electrode positions are crucial when developing an ECG that can be used reliably and safely by laymen.

However, since large-scale experiments and measurements are needed for said research, the availability of a mathematical simulation model simplifies this process significantly compared to conventional testing on human subjects. One advantage of using a mathematical model for testing is that the influence of modifications to the setup can be reviewed almost in real-time. This makes tests and systematic adjustments more practicable which then results in more efficient test series in general. Additionally, without having to rely on the accessibility of human test subjects, the development and theoretical testing can be performed in a more independent

and reproducible manner because the simulations are not subject to the disturbances of the environment that arise when testing on actual subjects. Furthermore, computational models are not necessarily inferior to actual test subjects when considering abnormalities and pathologies because they allow for including patient-specific anatomies as well as simulating various diseases and pathologies within the heart. Although this is only a brief overview of how computer simulations can improve the efficiency of product research and testing, their importance becomes apparent.

1.2. Question and Objectives

The results of this paper are supposed to contribute to the overarching goal of developing a simulation model of the human thorax which simulates the electrophysiological processes of the heart and their propagation across the thorax to the body surface. Subsequently, the signals are supposed to be gathered by virtual electrodes and used to calculate the resulting body-surface ECG.
While thorough research on this topic has already been carried out in a previous thesis, the present results are not yet sufficiently accurate for practical applications. Therefore, the aim of this paper is to build on the existing research in order to improve the results. A resulting model is supposed to accurately represent the cardiac electrophysiology under physiological conditions, but also provide the opportunity to incorporate pathophysiological or patient-specific conditions later on. An example for this is the integration of patient-specific geometries of the heart into the model building process, meaning the incorporation of CAT- or MRI-scan files of a specific heart as a template for the geometry.

Considering the complexity of the field of research and the software that is utilized, the objective of this paper is confined to develop a reliable and stable simulation of the electrophysiology of the heart exclusively. This constraint is stated because the heart model is the source of all signals and therefore the most important part of a complete thorax simulation. Also, the process of developing the heart-model is very time-consuming because it is subject to a tremendous amount of variables, parameters and settings that need to be evaluated and adjusted individually. Therefore, the primary objective of this paper is set to focus on the thorough development of a reliable and stable simulation of the heart’s electrophysiology with the focus on an efficient computational performance. Nevertheless, the theory behind the development and coupling of the torso model will be described and incorporated into the workflow when convenient, in order to establish a starting point for the implementation of the torso in future research.

1.3. Approach

The previous project (in the following often referred to as “FHN model”) already developed a simplified model of a human heart and thorax, using the finite element method (FEM) software COMSOL Multiphysics [2]. Its model is based on the FitzHugh-Nagumo equation and produces reliable outputs. However, the outputs are not yet satisfactory in terms of accuracy compared to actual ECG results.
This thesis will evaluate whether the previous approach can be further optimized in order to improve its results or whether the pursuit of a different approach might be more convenient. In case of the latter, the goal is to implement a new model based on more appropriate equations in order to achieve the desired results.

The approach to address the previously described objective of this thesis is subdivided into several steps, with the first one being an intensive literature research. This includes research on the underlying biological, mathematical, and electrophysiological fundamentals (see chapter 2.2) on one hand and the current state of the art in cardiac modelling on the other (see chapter 2.1). The most important aspects will briefly be summarized in order to provide a quick overview of them. This mainly serves the purpose of recapitulating the basic fundamentals and terminology. For a more in-depth description of these topics, cross-referencing with further technical literature is recommended as in-depth explanations of each topic would exceed the scope of this paper at this point.

Due to the results of the literature research and the assessment of the FHN model, the decision to develop a new model based on the Aliev-Panfilov equations is made and pursued in the course of this paper. Because this process is very time-consuming and is supposed to be conducted as thoroughly as possible in order to obtain a model that is suitable for practical applications later on, the focus lies on the development of the heart model and its detailed description. This includes all steps of the model building process, from setting up the geometrical model and the mesh, assigning and implementing the appropriate equations and conditions, to fitting parameters, and adjusting the study settings. The coupling with the torso, however, will be referred to when appropriate but not pursued as a main goal. This is because the coupling itself has already been described and successfully presented in the previous thesis and is less complex to implement when regarding the development of the whole heart-torso model.
Therefore, the focus lies on the development of the heart model, which steps and their results will be described in the following chapters of this thesis.

2. Theoretical Background

2.1. State of the Art

The field of cardiac electrophysiology has started with the examination of excitation in simple one-dimensional nerve cells from where the knowledge was transferred to myocardial cells [3, 4]. Based on this foundation, various increasingly advanced models were presented and, with the simultaneous progress in computer technology and simulation software, developed to highly sophisticated simulations of the heart's electrophysiology [5–7]. Within the last decade even more complex electro-mechanical heart models, that couple the electrophysiology of the excitation with the mechanics of the contraction, were presented and brought the current state of research even closer to the goal of generating patient-specific, fully coupled whole-heart models [8, 9].

As a result of the increasingly detailed and realistic simulations being available, the field of application of cardiac electrophysiology has expanded over the years and includes a wide range of applications. Including, but not limited to, research of arrythmias and other pathologies in clinical cardiology [10], assessment of the impact of pharmaceuticals in drug development [11], design and optimization of medical devices and implants in biomedical engineering [12], and educational purposes.

2.2. Cardiology

While the main part of cardiac modeling is based on mathematical equations and the physics of electrical conductivity, the knowledge of cardiac anatomy and physiology is of great importance as well. The knowledge of the heart's anatomy is crucial for the development of a realistic geometrical model and especially for its simplification. When deciding which geometrical characteristics of the complex model can be omitted in order to simplify it while still preserving its key features, a profound understanding of the underlying anatomy is of great importance.

Similarly, the understanding of the heart's electrophysiology is of importance when the physics of the model will be implemented.

In order to provide a brief overview of these topics, the key aspects of each topic that are of importance in the course of this thesis will be described in the following chapters.

2.2.1. Anatomy

The human heart is located in the mediastinum with approximately 2/3 of its area on the left and 1/3 on the right side of the thorax, embedded within the lungs and the diaphragm. Its weight accounts for roughly 0,5% of the bodyweight.
On the inside, the heart can be divided into four cavities. The cavities on the left side of the heart (left atrium and left ventricle) are allocated to the circulatory high-pressure system, whereas the right atrium and right ventricle belong to the low-pressure system. This differentiation originates in the direction of blood flow as the right ventricle ejects the blood into the relatively small pulmonary circulation whilst the left ventricle needs to eject the blood into the aortic arch with a sufficiently high pressure to supply the whole systemic circulation (see Figure 1). [13]

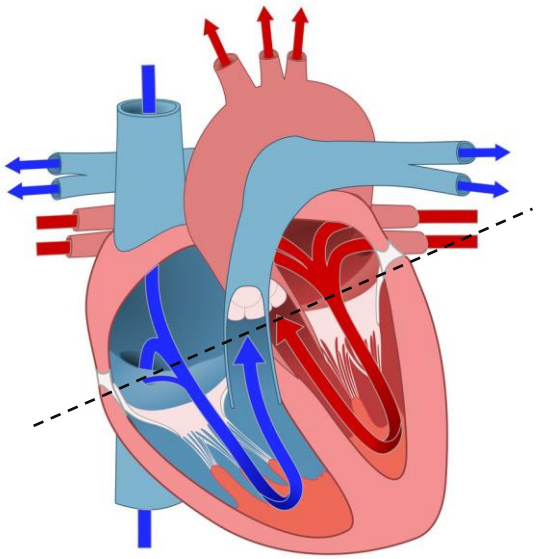

Figure 1: Direction of blood flow in the heart [14]

Also visible in Figure 1 are the four valves that regulate the blood stream within the heart. All valves are located in one valve plane (indicated by the dotted black line) which also acts as an isolator for the electrical conduction between the atria and the ventricles.

The heart wall consists of four layers which are, from outside to inside, pericardium, epicardium, myocardium, and endocardium. While each layer has its own importance, the myocardium is the most interesting for the purpose of this thesis as it consists of specific muscle cells for conducting stimuli and contracting the heart. The exact functionality of this system will be described in the next chapter. Furthermore, the myocardium's wall thickness

highly depends on the pressure ratio in the different chambers which is why a difference in wall thickness by approximately factor three presents between the left and right ventricle. [13]
Another important characteristic of the heart's tissue is the strongly anisotropic behavior. Due to significantly different conduction speeds depending on the fiber direction, signals move substantially faster along fibers than across them which leads to a coordinated excitement of the whole myocardium. [15, p. 568]

2.2.2. Electrophysiology

As mentioned in the preceding chapter, the myocardium consists of specialized muscle cells that serve multiple purposes. These cells can be separated into two groups, the first one being the cells of the working myocardium that are responsible for the mechanical work of the heart and therefore the contraction of the muscle [16]. A crucial characteristic of the myocardial tissue is the absolute refractory period of atria and ventricles. It describes the time span after the excitation of the muscle in which the tissue is not able to respond to further stimulation and therefore is not excitable within this period. This is a very important characteristic of the tissue as it ensures that the myocardium does not get stimulated and contracts in an uncoordinated manner which would likely result in fibrillation and an insufficient blood supply to the body and the heart itself. [17]

The second kind of cells belong to the electrical conduction system of the heart. It consists of the sinoatrial node (SAN), atrioventricular node (AVN), His bundle, left and right bundle branches, and the Purkinje fibers. The SAN is able to trigger the excitation by generating an action potential without any external input and therefore acts as the primary pacemaker of the heart. Although subsequent parts of the conduction systems have the ability to function in the same way, the SAN outperforms them due to its higher frequency of action potentials.
The excitation moves from the location of the SAN in the top right atrium to the AVN while activating the working myocardium of both atria. This results in their contraction which moves the blood from the atria to the ventricles. When reaching the AVN, the excitation is delayed in order to coordinate the activity of atria and ventricles. Given that the AVN is located in the valves plane which acts as an isolator, the excitation can only move on to the ventricles by passing through the AVN. From there, the excitation travels through the His bundle and the two bundle branches to the Purkinje fibers which pass it on to the cells of the working myocardium, leading to the contraction of both ventricles, starting from the apex of the heart. [16]
An overview of the different sections can be seen in Figure 2.

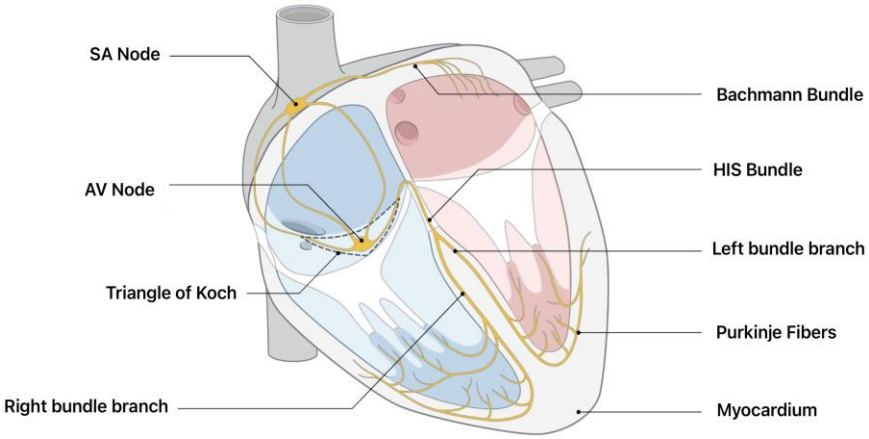

Figure 2: Electrical conduction system of the heart [18]

Each component in this cascade has different characteristics and conduction speeds which are listed in the following table:

Location	Intrinsic Rate	Onset	Speed
SAN	60-100 1/min	0 ms	0.05 m/s
Atrial Myocardium	-	85 ms	0.8-1 m/s
AVN	40-55 1/min	50 ms	0.05 m/s
Bundle of HIS	25-40 1/min	130 ms	1-1.5 m/s
Bundle Branches	25-40 1/min	145 ms	1-1.5 m/s
Purkinje Fibers	25-40 1/min	150 ms	3-3.5 m/s
Ventricular Myocardium	-	180 ms	1 m/s

Table 1: Conduction speeds [based on [16, p. 207]]

When measuring the excitation as voltage over time, characteristic action potential shapes can be identified, depending on the location of measurement. A general overview of the morphology of these signals can be seen in Figure 3:

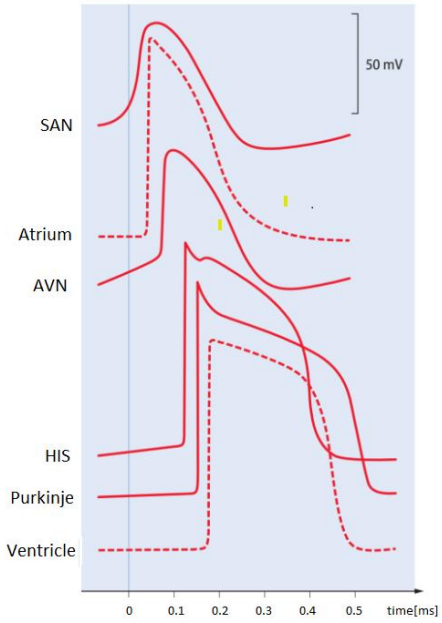

Figure 3: Action Potential shapes [17, p. 194]

2.2.3. Electrocardiogram

In order to illustrate the electrical activity of the heart, an electrocardiogram can be used. The technique is based on the fact that electrical potential differences that occur during the heart's excitation propagate through the thorax and can be measured on the body surface with electrodes. The electrocardiograph then amplifies and filters the measured signals in order to evaluate and display them in various forms.

One way of processing the gathered signals is to sum them up and plot them as a resulting vector loop. This vector loop consists of the sum of all individual potential vectors that occur when excitation propagates along the myocardium. [16, p. 208]

A different way of visualizing the signals is to plot the vector's time-dependent progression in relation to different planes, so that the plotted amplitude is dependent on the plane of consideration. Said planes are better known as ECG leads, most commonly used in terms of limb leads and chest leads. Each lead is depicted in the ECG as a distinct curve that graphically represents the amplitude of potential differences between two or more electrodes in millivolts as a function of time.

Depending on the purpose of the examination, different ECG-lead systems can be applied, varying in the number of leads and consequently in the level of detail of the results. The most common ones are the Einthoven, Goldberger and Wilson lead system which are based on different numbers of limb- and chest leads.

A very common basic type of ECG is the six-lead ECG which is based on only three electrodes applied to the limbs of the patient. As this is a comparatively easy to use yet significant technique it is often used for basic monitoring or long-term ECG examinations. However, since it is based on only three electrodes it's validity and significance regarding extensive cardiological diagnostic is limited.

The six-lead ECG can be divided into two systems that are both based on the same three limb electrodes on the right and left arm (RA and LA) and the left leg (LL). Often an additional fourth electrode is applied to the right leg for grounding. The first system is called the Einthoven system and generates the three most evident limb leads, Einthoven I, II, and III, by calculating the differences between two electrodes. This can be seen in the top row in Figure 4.

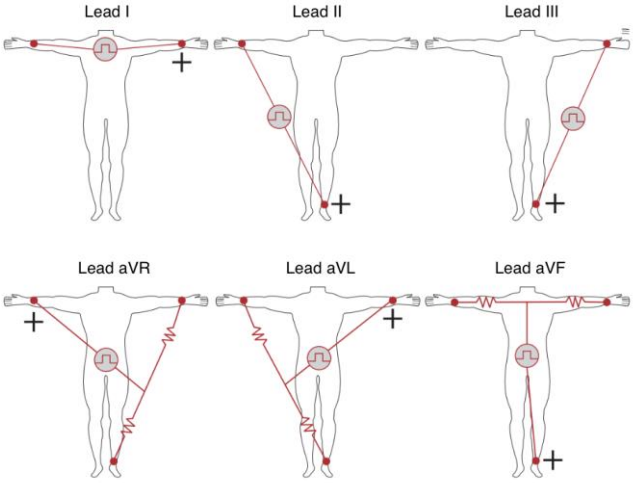

Figure 4: Einthoven and Goldberger Leads [19]

The corresponding equations for calculating the three Einthoven leads are the following [20]:

$$I = LA - RA$$
$$II = LL - RA$$
$$III = LL - LA$$

Eq. 1

The second system of the six-lead ECG is the Goldberger system which adds three additional, augmented limb leads (aVR, aVL, aVF) that stand orthogonally to the Einthoven leads. This is displayed in the bottom row in Figure 4 and mathematically described by the following formulas [21]:

$$aVR = RA - \frac{LA + LL}{2}$$
$$aVL = LA - \frac{LL + RA}{2}$$
$$\mathrm{aVF} = \mathrm{LL} - \frac{\mathrm{RA} + \mathrm{LA}}{2} \qquad \text{Eq. 2}$$

When more detailed results are needed, six additional electrodes on the chest, also known as chest- or Wilson leads (V1-V6), can be applied and provide the user with a more detailed view of the heart's electrical activity. Their calculations are based on the three electrodes of the six-lead ECG and are extended by the additional six electrodes on the chest. This combination of Einthoven, Goldberger, and Wilson system produces twelve leads and is therefore commonly referred to as 12-lead ECG and nowadays the standard examination technique in cardiology. The placement of the electrodes for the Wilson leads can be seen in Figure 5, where the blue electrodes indicate the locations for the standard 12-lead ECG. Sometimes extending the field of interest to the right side of the chest may be necessary in which case the electrodes can be applied as shown in the positioning of the red electrodes. This enables the evaluation of the heart's electrical activity from a different angle and can be useful for diagnostic purposes.

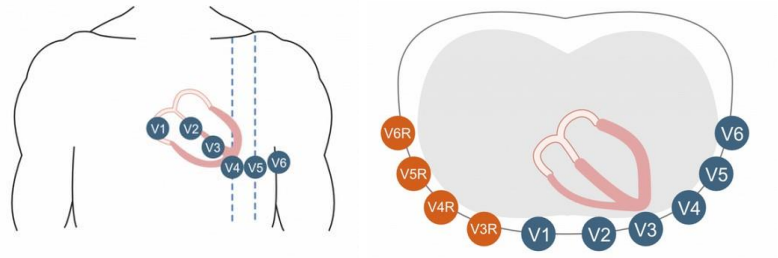

Figure 5: Electrode Positioning 12-lead ECG [19]

The calculation of these leads is based on the potential difference between one chest electrode and the so-called Wilson central terminal which is considered an arithmetical mean of the three limb leads [22]. This leads to the following formulation:

$$V_i = \varphi_{Vi} - \frac{RA + RL + LL}{3} \qquad \text{Eq. 3}$$

where $\mathrm{V_i}$ stands for one of the six Wilson leads and φ_{Vi} for the potential at the corresponding electrode.

2.3. Mathematical Approach

The task of deriving an ECG on the virtual surface of a computer model that simulates the cardio-electrical activity is commonly known as *forward problem* of electrocardiography. The challenge in solving this problem is to develop suitable mathematical models that display the physiological conditions in a sufficiently detailed yet computationally efficient manner [15].
Simple approaches that illustrate the heart muscle as a whole are often not detailed or precise enough for using the results in a scientific manner. In order to increase the level of detail of the simulation and therefore the solution, multiscale approaches can be used that integrate the solution over various domains. Regarding the aim of this project, this means that the computation considers most of the domains that are affecting the solution. A schematic explanation of this principle can be found in Figure 6.

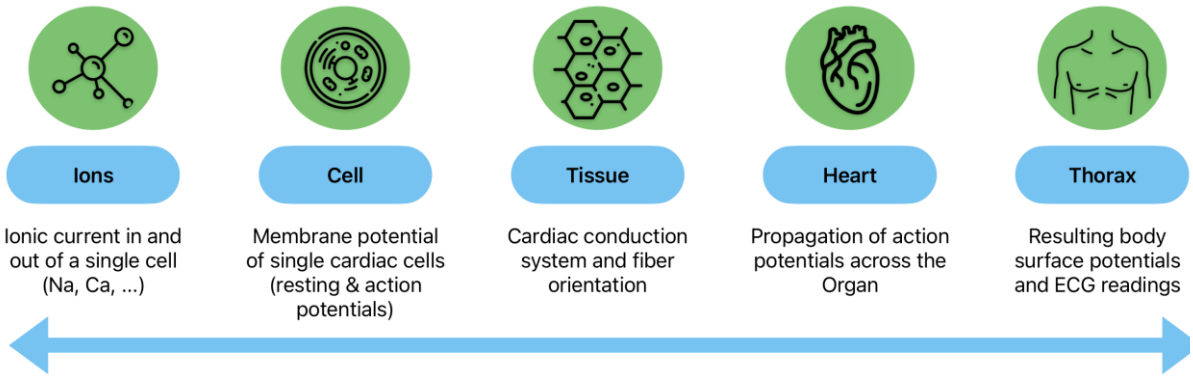

Figure 6: Multiscale Approach [own image]

Several mathematical approaches for describing the electrophysiological activity of the heart have been developed and validated in the past. Depending on the domain, the desired solution, and the given circumstances (e.g., computational resources available), the best-fitting model can be chosen individually for every simulation. The most common models and their characteristics will briefly be presented in the following sections.

2.3.1. Ionic Models

Almost all models that describe the electrophysiology of the heart start at the very beginning with the description of the total transmembrane current that can be measured at the membrane of the cells. Depending on the type and detailedness of the model, various equations are set up in order to describe the current either physiologically as a sum of the individual ionic currents, or phenomenologically as equations that describe the integral characteristics of the

underlying physiology. Regarding the desired level of detail and the computational load, various models are available and can be chosen accordingly.
The commonality of all models is the consideration of the cell membrane as a circuit in which the ionic current and a capacitor are connected in parallel in order to represent the total transmembrane current. This is represented in the following Eq. 4.

$$I_m = C_m \frac{\partial V}{dt} + I_{ion} \qquad \text{Eq. 4}$$

In this formulation, $\mathrm{I_m}$ denotes the total transmembrane current, $\mathrm{C_m}$ the membrane capacitance, and V the transmembrane potential, in this case as change over time. $\mathrm{I_{ion}}$ stands for the equations that are used to describe the ionic currents or their behavior and is the crucial term for the complexity of the model. [23]

Extremely detailed physiological models are for example the Courtemanche-Ramirez-Nattel (CRN) [24] model for atrial cells and the ten Tusscher-Noble-Noble-Panfilov (TNNP) [25] model for ventricular cells. Both of these models describe the individual ionic currents to great detail and are therefore highly suitable for cases that examine the heart's behavior on ionic levels, such as studies on the effects of changes in ion concentrations. To this day there are several models and their variations available that fundamentally rely on the same principle, but differ in the multitude of observed ionic currents and therefore in their complexity. While these kind of models are extremely accurate, they are inefficient in terms of computational power, due to the large number of combined equations that they are based on. In case of the CRN model for example, the transmembrane currents are represented by 12 gating variables and up to 59 ordinary differential and algebraic equations need to be solved. Usually, the formulation for these models resembles the example in Eq. 5 which is taken from the CRN model and exemplifies the composition of the equations that describe the ionic currents.

$$I_{ion} = I_{Na} + I_{K1} + I_{to} + I_{Kur} + I_{Kr} + I_{Ka} + I_{Ca,L} + I_{p,Ca} + I_{NaK} + I_{NaCa} + I_{b,Na} + I_{b,Ca} \qquad \text{Eq. 5}$$

Each of the individual currents ($\mathrm{I_{Na}}$, $\mathrm{I_{K1}}$, …) is yet again represented by multiple differential and/or algebraic equations, accounting for the complexity of these models. [24]

In the interest of striking a balance between reducing the computational load and maintaining results of sufficient quality, models with a significantly reduced number of gating variables and

consequently fewer differential equations can be used. Models of this type are often referred to as Hodgkin-Huxley-type models (HH), named after the mathematical description of excitability in cells posed by Alan Lloyd Hodgkin and Andrew Fielding Huxley in 1952 [3]. The simplification of these models occurs through a reduction of the considered currents to those that are responsible for the key characteristics of the excitation. In case of the HH model, only sodium and potassium currents are considered along with a third variable whose purpose is to combine the remaining currents. The original HH formulation is shown in Eq. 6 [3].

$$I_{ion} = C_m \frac{dV_m}{dt} + g_K n^4 (V_m - V_K) + g_{Na} m^3 h (V_m - V_{Na}) + g_L (V_m - V_L)$$

$$\frac{dn}{dt} = a_n (1 - n) - \beta_n n \qquad \text{Eq. 6}$$

$$\frac{dm}{dt} = a_m (1 - m) - \beta_m m$$

$$\frac{dh}{dt} = a_h (1 - h) - \beta_h h$$

Compared to Eq. 5 significantly less variables and equations are used to describe the ionic currents which leads to a simulation that is less precisely adjustable yet considerably more efficient regarding computational power. Based on this formulation, several derived models have been proposed during the years which is why a large number of models are available to choose from for each specific purpose and field of application.

2.3.1.1. FitzHugh-Nagumo Model

One of the simplest models of HH-type is the FitzHugh-Nagumo (FHN) model which reduces the HH model down to only two gating variables, a fast and a slow one, see Eq. 7 [26].

$$\frac{dv}{dt} = v - \frac{v^3}{3} - w \qquad \text{Eq. 7}$$

$$\frac{dw}{dt} = v - a - bw$$

This model is often used due to its simplicity, although it does have its challenges regarding the adaptability of the simulation. Due to the lack of variables, only few adjustments can be made to adapt the model to the needed specifications.

To overcome this constraint, several adaptions of the model were represented in the past such as the one developed by Dokos et al. [27] in 2007. This model presents an approach to generate action potentials by the use of modified FitzHugh-Nagumo equations with several additional parameters compared to the original model. Eq. 8 [27] shows said equation in the formulation for the atrial region.

$$\frac{\partial u}{\partial t} = \nabla.(\sigma \nabla u) + kc_1(u-B)\left(\frac{u-B}{A} - a\right)\left(1 - \frac{u-B}{A}\right) - kc_2 v(u-B)$$
$$\frac{\partial v}{\partial t} = ke(\frac{u-B}{A} - dv - b) \qquad \text{Eq. 8}$$

Compared to the original formulation, several additional parameters have been introduced in this equation which correspond to various characteristics of the model and can be used to adjust them accordingly.

2.3.1.2. Aliev-Panfilov Model

Similar to the FHN model, the Aliev-Panfilov (AP) model is of HH-type and a two-variable model as well. It improves on certain flaws of the FHN model, for example the failure to reproduce the accurate shape of action potentials and other important features [28]. The equations look somewhat similar as they describe a slow and a fast process as well:

$$\frac{\partial u}{\partial t} = \frac{\partial}{\partial x_i d_{ij}} * \frac{\partial u}{\partial x_j} - ku(u-a)(u-1) - uv$$
$$\frac{\partial v}{\partial t} = (\varepsilon_0 + \frac{\mu_1 v}{u+\mu_2})(-v - ku(u-a-1)) \qquad \text{Eq. 9}$$

The anisotropy of the heart tissue is included in this equation by the conductivity tensor d_{ij} while *k*, *a*, and ε_0 are set and μ_1 and μ_2 are for adjustments later on. Since the variables *u*,*v*, and *t* are dimensionless in this formulation, they need to be rescaled in order to describe the actual transmembrane potential and time:

$$E[mV] = 100u - 80 \text{ (transmembrane potential)}$$
$$t[ms] = 12.9t[t.u.] \text{ (time)} \qquad \text{Eq. 10}$$

With the use of these equations, the restitution properties of the cardiac tissue can be described more accurately than with the previously described FHN model.

2.3.2. Tissue Models

Once the electrical behavior of a single cell has been described with one of the models mentioned above, the spatial propagation of said signal across cells needs to be modeled. This is also known as cellular coupling and leads to a result that incorporates both spatial and time domain [15, p. 553].

Single cells are interconnected via gap-junctions which couple adjacent cells and enable a fast transmission of action potentials across the tissue [29, p. 28]. This leads to a very complex and detailed structure which is almost impossible to represent by equations which is why the structure of the tissue often gets homogenized. This simplifies the computation tremendously while still producing adequate results for most purposes [15, p. 566]. There are two well-known models that can be used to approximate the structure of the tissue which are the mono- and bidomain model.

The bidomain model is the more complex version of the two because, as indicated by the name, it considers the composition of cardiac tissue as two domains. These domains are the intra- and extracellular space, separated by the cell membrane where the transmembrane potential arises. When calculating with the bidomain model, both domains are considered to be intertwined, meaning that each point in space is considered to consist of both intra- and extracellular space. This assumption leads to a detailed description of the cardiac tissue and its electrical behavior but is computationally demanding in terms of computational load when performing simulations [15, p. 567].

To avoid computation costs, the assumption of equal anisotropy ratios can be made which reduces the bidomain to the monodomain model. This assumption does simplify the underlying physiology a lot while still leading to sufficiently accurate results for most purposes [30].

3. Model Building Process

The process of developing a model in the course of this thesis started nonbiased and open to any kind of model. To begin with, every approach was considered possible, from maintaining and improving the existing FHN model of the previous thesis up to the point of implementing a completely new model from scratch. In the course of assessing the field of mathematical cardiology as well as the previous thesis, the decision to revert to a different model rather than the FHN model was made and will be further evaluated on in the following chapters. In the process of deciding on a new model to base the simulation on, several different models have been evaluated, from very complex ones such as the TNNP up to highly simplified models of HH-type. While complex ion-based models in the style of the TNNP model were quickly deemed unfit to the purpose of this paper due to their complexity and expected computational load (up to 50 ODEs in some cases), the focus was set to models of HH-type. During the evaluation of various models, particularly the AP-model singled itself out due to the expected quality of its results in combination with a low number of parameters and a comparatively low computational load. Supported by a wide range of available literature on the theory of this model, the choice for the implementation of the Aliev-Panfilov model was made.

The implementation of a simulation that is based on the fundamentals of the AP model rather than the FHN model was an extensive task which included a lot of research and trial runs. While the basic outline of the model building and corresponding decision-making process for this simulation is described in this section, the elaboration on the specific components and their exact details will be presented in chapter 4. In order to put the individual steps into context and to provide a scheme for better understanding of the procedure, the basic composition of the simulation will be described briefly in this chapter.

The mathematical core of the simulation is based on the equations of the Aliev-Panfilov model, which describe the electrical activity of myocytes in the heart. The geometrical model that these calculations are projected on within the FEM environment is a semi-detailed, three-dimensional computer aided design (CAD) model whose measurements and properties are based on the anatomy of an actual human heart (see Figure 8). This geometry is divided into the different sections of the electrical conduction system (SAN, AVN, …) so that the parameters can be adjusted for each region individually. This heart-geometry itself is again embedded in a coarser structure that represents the human torso. This geometry is less detailed than the heart, yet still covers the most important anatomical features of the torso such as its shape and the position of the lungs.
These two main sectors, heart and torso, are divided into several smaller regions, depending on the material that they are made of or contain. In this case, blood, heart tissue, lung tissue,

an isolator and the chest-region in general are divided and allocated to selections. For each selection, individual material properties can be defined. Especially the electrical conductivity and the relative permittivity which are crucial for the simulation of the conductibility of electrical currents within the model are of importance. In order to pass the action potentials from the heart on to the surface of the torso, the physics of heart and torso are coupled mathematically.

A general overview of this schematic structure of the simulation as described previously can be seen in Figure 7 below.

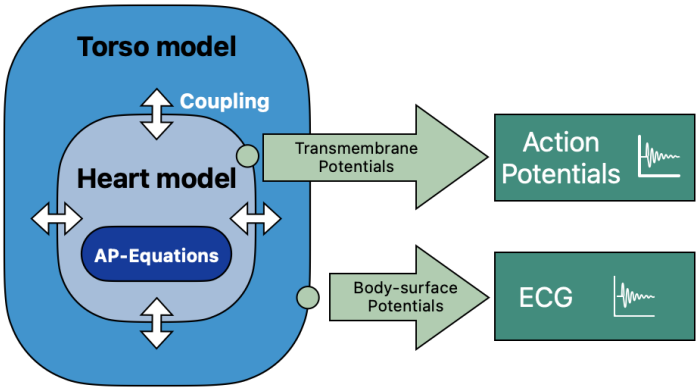

Figure 7: Simulation Scheme [own image]

3.1. Materials

The materials that were used throughout the research on this paper are described in this section. This includes a description of the previously conducted thesis on this topic as well as a brief introduction to the software that has been used.

3.1.1. Previous work

A previous thesis that worked on simulating the electrophysiology has been presented in 2022, coming up with an approach that utilizes the FHN model [31]. Simulations are conducted in a multiphysics FEM software on a simplified 3D geometry of the human heart that reduces the heart to a basic four-chamber model while still maintaining important anatomical features such as the difference in wall thickness between the left and right ventricle.
Regarding the mathematical part of the preceding thesis, the FHN model as modified by Dokos et. al. [27] was employed to simulate both atrial and ventricular action potentials. Despite numerous attempts to adjust the parameters in a way that the generated action potentials correspond to those in the literature, the results are not yet sufficiently robust enough for

practical applications. Further details on this can be found in the aforementioned thesis, however, key aspects will briefly be summarized here to facilitate comprehension of the subsequent steps in this paper.

A main issue with the given simulation based on the FHN model is that several individual ventricular action potentials do not match with their expected physiological shapes which necessitates further adjustments to their corresponding parameters. The difficulty with this task lies in the fact that the behavior of parameters no longer follows a linear pattern given the complexity of the model, which makes the task of predicting suitable parameters and their combinations very difficult and time-consuming. This situation is aggravated by the fact that a single simulation (equivalent to 1000 ms of simulated time) with this model takes approximately 25 minutes, thereby limiting the throughput of simulations and parametric sweeps. Although a variety of parameter combinations were tried to improve the situation, no satisfactory solution was to be found within the given processing time.

Hence, a thorough assessment of the previous paper and its accompanying documentations was conducted in order to decide if further attempts of optimization appear reasonable or whether the implementation of a different model might be the better alternative. This involved a complete reassessment of the presented program including the chosen geometry and mesh, the implementation of the underlying differential equations and parameters, and the chosen study settings.

The assessment of the geometry did not give reason to doubt its practicality as it is based on and very close to the anatomy of an actual human heart, both in measurements as well as in its basic structure [31, 32]. Furthermore, several other papers that conducted similar research to this study used comparable or even further simplified geometries with at least satisfactory results in most instances [7, 33, 34]. The same is the case for the utilized mesh, which does not appear as a critical source of error in the present simulation.

Since the key component and therefore the most likely source of error in this kind of simulations is the implementation of the physics, here represented by the exertion and coupling of the various differential and algebraic equations, the assessment was focused on reevaluating this stage of the model-building process. Thereby, the main focus of attention was on the alteration of the corresponding parameters which was conducted with the use of COMSOLs parametric sweep function as this function allows for processing parameters as ranges. This enables the coverage of multiple value-alterations for one parameter and even combinations of several varying parameters in one simulation, making the examination more efficient and the results easier to compare. These alterations have already been performed at great length within the scope of the model development and were documented in detail. A review of this documentation did not give reason to assume that crucial points were missed or that further

attempts to adjust the parameters were to be successful within the near future, especially when considering the long computing time for a single simulation.

Due to the lack of promising results from the reassessment of the present model in combination with the results of the literature research which suggest that other models might be superior to the FHN model for the purpose of this study, the decision to neglect the FHN approach and to implement the AP model was made.

3.1.2. COMSOL Multiphysics

The main software utilized for simulations in this paper is COMSOL Multiphysics, Version 6.0. As implied by its name, COMSOL Multiphysics is a simulation environment based on the finite element method (FEM), that enables users to perform simulations not only on single-, but also on fully coupled multiphysics models. [2] Being able to couple as many physics together as needed is of great importance for the handling of this paper's problem, as it allows for connecting the mathematical description of the ionic currents in form of partial differential equations (PDEs) with the electrical behavior of the heart's conduction system in form of electric currents. This coupling can conveniently be handled with the use of the *General Form PDE* and *Electric Currents* physics interfaces that are provided within the software.

When creating simulations, COMSOL itself can serve as a stand-alone tool for creating fully functioning models. This includes building and meshing a geometry, defining material and physical properties, adjusting the solver specifications, and drafting the desired output tables and graphs. The whole process is supported by several integrated tools and features such as the Model Builder, Model Manager and Application Builder that guide the user through various steps, facilitating the model-building process as much as possible. [2]
While most of these tools are very extensive and sufficient enough to create even highly complex simulations, the provided geometry tools and operations can be inconvenient to use, especially when working with complex, asymmetrical structures. In these cases, additional software for designing and potentially also meshing the geometry may be considered since COMSOL allows for the import of external geometries and meshes. This will be further elaborated on in chapter 3.2.1.

Regarding the user-friendliness, COMSOL offers a vast amount of knowledge and information on their product and the underlying physics online which can be useful for understanding and building simulations in addition to the already built-in help and documentation [35, 36].

3.2. Geometry and Meshing

As mentioned above, the geometry that was developed in the course of the preceding thesis appears suitable for its purpose and has been adopted for the implementation of this simulation. The same applies to the existing torso model which was transferred to this model as well. Both geometries will briefly be described in this section.

To allow for a better representation of the different regions of the heart, the geometry was divided into various domains that represent important regions such as the SA- and AV-node or the Purkinje fibers for example. This division is mathematically relevant because parameters can be defined for each domain individually which leads to customized results depending on the region. Figure 8 shows a cross section of the heart-geometry along with the representation of the different domains that were defined and the position of the corresponding measuring points within them (red marks).

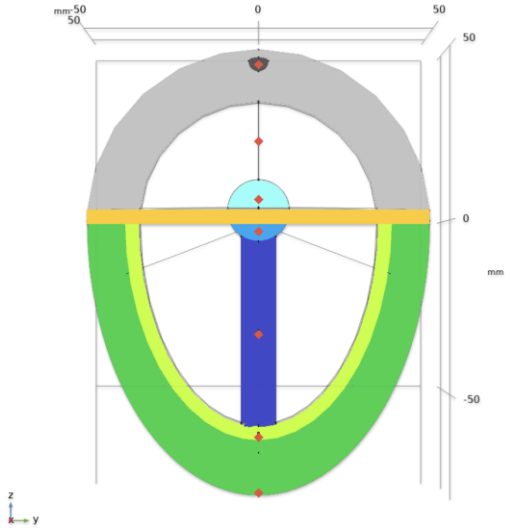

Figure 8: Structure and domains of the heart-geometry [own image, based on [31])

(Light grey: atrium, Dark grey: SAN, light blue: AVN, orange: valvular plane, blue: HIS bundle, dark blue: bundle branches, light green: Purkinje fibers, dark green: ventricle myocardium, white: heart chambers)

Unlike depicted in the figure above, the hearts anatomical position within the chest is not upright, but slightly tilted. Nevertheless, in this application scenario the geometry is built to be aligned with the coordinate axes as this allows for the manual mapping of points within the heart using the three spatial coordinates (X,Y,Z). Additionally, measurements can be described in a more convenient way when the geometry aligns with the axes. Rotation will be introduced later on in the model building process.

The heart-geometry itself is embedded in a significantly simpler, yet still anatomy-based torso environment that simulates the lungs and chest. This coarse torso model mainly acts a conductor for the electrical impulses that are generated within the heart, so that the signals can be read on the simulated chest-surface in order to calculate the ECG leads. This is why the torso model is supposed to approximate an actual human anatomy to a certain extent, but is not required to display an elaborate level of detail, especially as this would increase the computational load which is not necessary in this stage of the development of the simulation. Figure 9 shows the geometry of the torso and the virtual ECG electrodes of the Wilson leads on the surface of the chest.

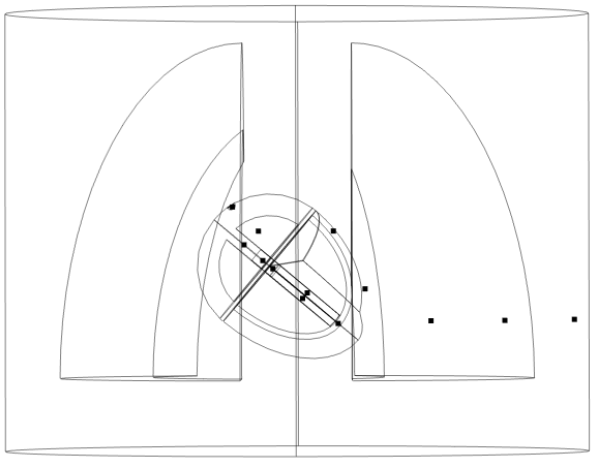

Figure 9: Structure of the torso-geometry [own image, based on [31])

Regarding the meshing, heart and torso will be treated separately which can easily be implemented in COMSOL by creating as many meshes as needed and assigning the different domains accordingly. In this case, two main tetrahedral meshes are created that mesh the heart and torso independently. When assigning a mesh to a domain, COMSOL calculates a standard, preliminary mesh for the designated area. Although this mesh might be already sufficient without any further optimization, a mesh refinement process should be performed in order to obtain an impression of the solutions convergence respectively. In a very basic form this means that several simulations are performed consecutively, starting with a very coarse mesh that is incrementally refined. The solution of each simulation is then evaluated and judged by comparing it to its previous result, obtaining an impression of the convergence depending on the mesh size. The decision of whether the model can be considered converged depends on the judgment of the user. Typically, at least three solutions are observed until the variation between the solutions becomes small enough to be considered insignificant by the user. The obtained mesh can then be further adjusted or used for the simulation, as the refinement process increases the confidence in the model and therefore the results. [35]

The following development of the simulation was performed on a simplified version of the model which only considered the heart model and not yet the coupling with the torso. This was considered reasonable for this purpose because, as mentioned above, the primary success of the model was measured on the generated action potentials and not the conduction of said signals to the body surface. Therefore, neglecting the torso model leads to a significantly reduced computing time without impairment of the results at this point.

3.2.1. Patient-specific Geometry

For all calculations in this paper, the geometry as per chapter 3.2 was adopted. Nevertheless, the development of a patient-specific geometry was evaluated as it appeared of importance for further evolution of the simulation and a more realistic reference to an actual human heart. The goal of this was not only to receive a geometry that looks like an actual human heart rather than the approximated shape of the interim geometry, but also to elaborate a workflow that allows for incorporating individual morphologies of the heart, based on a specific patient.

The foundation for this are DICOM (Digital Imaging and Communications in Medicine) files which contain datasets from CAT- and MRI scans. The dataset of one scan contains two-dimensional images of each of the three main anatomical planes (coronal plane, sagittal plane, transverse plane) which can be viewed individually or combined as a 3D rendered image. For research purposes, several DICOM files are publicly available online on various platforms, such as Osirix [37], where the example file for this paper was obtained and used for further evaluations. The chosen file was a 16 detector CT scan of a healthy heart (Dataset “AGECANONIX” from the Osirix Dicom Image Library [37]) with mildly calcified coronary arteries which were neglectable in this case. Specifically, the systole-dataset was used which can specifically be distinguished because the CT-cycles are synced to the patient’s ECG and are therefore able to record each slice at the same phase of the heart cycle. Due to this technique, both a diastole and as a systole dataset of the heart are available and can be evaluated individually [38]. This file was used to generate a volume mesh, based on the specific anatomy of the patient to be imported in COMSOL and used for the simulations.

Preparation

This involved importing the DICOM file into a program for viewing and segmenting, in this case 3D Slicer (Version 5.6.1.) [39] which acts as a DICOM-reader on one hand and as a segmenting tool on the other. All three two-dimensional planes as well as a three-dimensional

image are constructed from the dataset and prepared for editing and segmenting (see Figure 10).

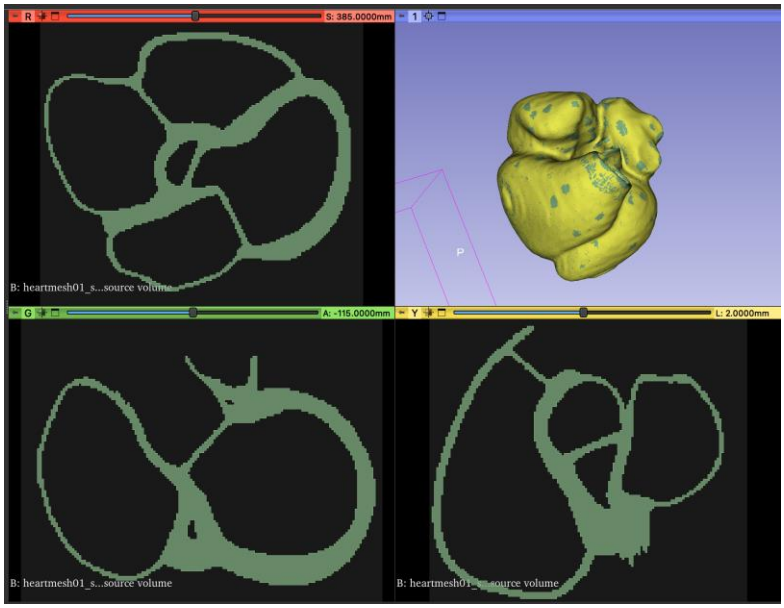

Figure 10: 3D Slicer [own image]

(Top left: transverse plane, top right: 3D-rendered image,
bottom left: coronal plane, bottom right: sagittal plane)

To begin with, the DICOM file (.dcm file format) was loaded into the software and a suitable view of the program windows had to be adjusted. As seen in Figure 10, all four views are visible and can be navigated individually which was important for delineating the heart muscle from surrounding structures.

This was performed by first adapting the threshold of Hounsfield-Units (HU) in a way that as much heart muscle and as few other structures as possible were visible in the selection. This led to a selection that included most of the heart muscle, but also a lot of other structures with similar HU-values. These were manually separated from the heart by using provided tools such as snipping, mark-up, and cropping tools until only the heart muscle was left (see Figure 10). This result served as an initial approach, but had to be further improved in order to receive a sufficient model. Improvements were made by filling holes and fixing segments with insufficient wall thickness as well as simplifying certain areas that were not correctly depicted in the first place and appeared as disruptions in the image (such as valve flaps or irregularities in the heart wall). Lastly, the remaining openings for vessels (aortic arch, vena cava, etc.) were closed and the whole selection was smoothed with a gaussian filter.

Segmentation

After the obtained results appeared sufficient in all four views, segmentation could take place. This was necessary in this stage of the development because there is no convenient solution for dividing complex non-symmetrical geometries into segments in COMSOL itself. In 3D Slicer, the segmentation was performed by selecting and dividing the individual areas such as the area for the SA and AV node, the approximate region of the HIS bundle and bundle branches, and so on.
Once the individual regions were segmented and labelled accordingly, the data was exported as wavefront files (.obj) in a way that each region corresponds to one .obj export file and could be opened individually.

Meshing

The next step was meshing the components that were segmented in the previous step. This required the use of another software tool that was able to open the wavefront file, mesh the components and edit the created mesh, if necessary. The software of choice was MeshLab (Version 2023.12) [40], an open source system for working with three-dimensional meshes.
When opening files in MeshLab, a mesh is generated automatically which can then be edited and adjusted depending on the needs of the user. In this case, the automatic mesh was extremely fine which was not suited for this purpose as this could lead to multiple issues later on, especially to overly detailed areas which result in an immense expenditure of computing power. Therefore, a simplification of the mesh was executed by means of a quadric edge collapse decimation algorithm. Afterwards, the mesh was cleaned up by removing duplicated vertices and edges and by closing holes.
These steps were repeated for all files which then were exported into STL files (.stl) that ultimately could be integrated into COMSOL as an imported mesh.

3.3. Equations, Conditions and Coupling

After defining the geometry and the mesh, the next step was the evaluation of the system of equations that describe the Aliev-Panfilov model and its conversion into a format that could be handled by the differential equations module in COMSOL. In this case the choice for the *coefficient form PDE* was made. Alongside with the formulation of the equations, boundary conditions as well as a primary set of initial values needed to be defined in order to obtain a first impression of the model's performance. While the initial values are based on the underlying physiology of the resting potentials and could be taken from the literature, the

boundary conditions needed to be chosen and adjusted based on the simulation. For this scenario, Neumann boundary conditions were chosen because they describe the flow of current across the membrane rather than the actual voltage as it would be the case with Dirichlet boundary conditions. This seemed to be a better fit for the purpose of this simulation and was therefore implemented, initially.
Depending on the results of this first simulation, the conditions had to be adjusted along with the evaluation of a suitable external stimulus that elicits the excitation. Once these steps led to a stable simulation, the adjustment of the parameters took place. This process was rather time-consuming and was conducted until a satisfying solution was found.

After the simplified version of the model was sufficiently adjusted, the coupling with the torso model was set up and integrated into the simulation, providing a groundwork for the incorporation of the torso model, later on. COMSOL offers a variety of possibilities for the coupling of physics and components. In this case the coupling via variables was chosen whose basic principle is illustrated in the following Figure 11:

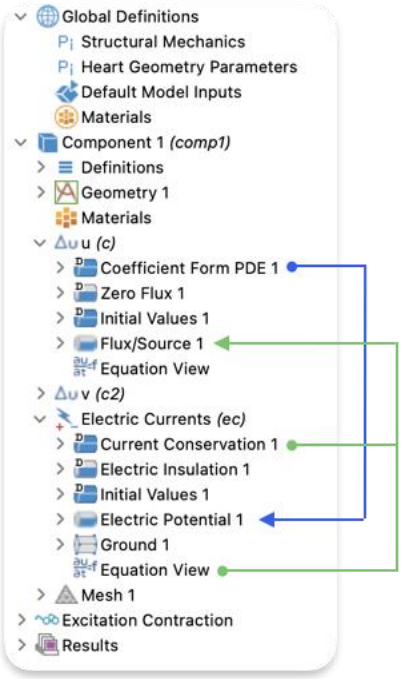

Figure 11: Schematic representation of Coupling [own image]

It shows the COMSOL model building tree and the two physics that are supposed to be coupled. The colored arrows indicate the communication between the individual components in form of variables. Thereby, both physics rely on input information from the respective other and are therefore dependent on one another.

3.4. Study Settings

Lastly, the study parameters were adjusted in order to improve the detail and computational load of the simulation. This was a crucial step especially for the performance of the whole simulation as the adjustments made in this section impact the handling of the equations and therefore the computational load significantly. The study chosen for this model is of a time-dependent type because the observed variables change over time. When adding the study node to the simulation, COMSOL automatically chooses a set of default settings for the solver which can be adopted without the need for changes when running the simulation for the first time. Changes should not be necessary until the simulation does not behave as expected [35]. The time stepping method of choice for the simulation is a backward differentiation formula (BDF) solver which is known for its stability. As per default settings, a maximum order of five and no restrictions regarding the time steps taken were introduced. This leaves the choice of timestep size up to the solver which tries to maximize the timesteps when possible while downsizing it to smaller increments, if necessary. This is usually the case when the variation of the solution starts to accelerate over time. This flexibility increases the efficiency of the solver.
In this case, the adoption of the auto-settings already led to a successfully compiled solution which is why the subsequent changes to the settings (described in chapter 4.4) were focused on optimizing the performance of the solver regarding its stability and efficiency.

3.5. Outputs

COMSOL offers a variety of possibilities to visualize the results of the simulation. Plots of any kind can be generated, from simple one-dimensional graphs to complex three-dimensional representations of the geometry or the mesh. The graphs can be adjusted freely, entirely depending on the needs of the user. Key components of the adjustment are besides the appearance (title, labels, legends, scale, etc.) the selection of the measuring points whose values are supposed to be plotted together with their expressions and units. Several different plots can be combined in a plot group and displayed in one graph by adding individually adjustable sub-nodes to the group.
For the different aspects of this simulation, different representations have been chosen. The visualization of the action potentials and the ECG leads is performed by generating a one-dimensional point graph as this allows for plotting the dependent variable (in this case the voltage) as a function over time. The action potentials are plotted for each domain individually at defined measuring points (see Figure 8, black dots). The ECG leads are calculated from specific points at the torso surface (see Figure 9, black dots).

The display of the spreading of excitation across the tissue of the heart model on the other hand is shown as color-indicated two-dimensional planes of the heart geometry. Meshes are displayed as a three-dimensional plot of either the volume or the surface mesh.

4. Results

4.1. Geometry and Mesh

The geometry is adopted as described previously without any additional changes. The mesh however is optimized by assigning individual mesh sizes for the torso and the heart which allows for the use of a coarser mesh for the torso and therefore a reduction in computing time. Both meshes are auto generated by COMSOL and then evaluated regarding their specifics and quality in case they need further refinements or improvements. The quality is assessed by regarding the skewness of the mesh which can be seen in the figure below, together with the plot of the respective meshes in the XZ-plane.

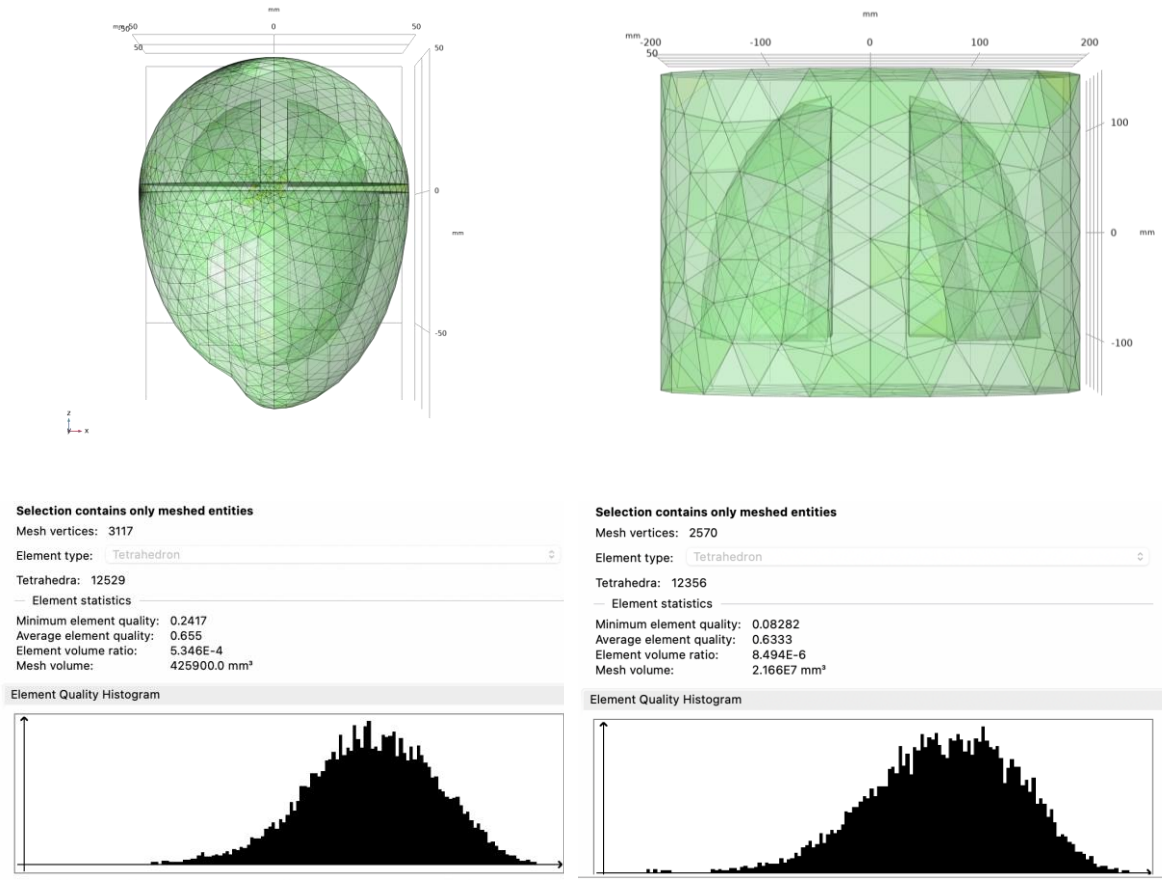

(a) Heart Mesh (b) Torso Mesh

Figure 12: Meshes and corresponding Properties [own image]

When looking at the plotted meshes at the top row, the size difference between the two mesh sizes becomes apparent. The fine heart mesh is significantly denser and more detailed than the coarse torso mesh by contrast. The histograms represent the mesh element quality measured in absolute values between 0 and 1, where 1 equals the best possible quality and 0

a degenerated element. The average element quality of the auto generated mesh lies above 0.6 in case of both the heart and the torso mesh.

The mesh refinement process was started with mesh size *coarser* and was refined until the solutions converged which was considered to be the case with a *finer* mesh size. The results of this process are presented in Figure 13 below. Because the evaluation of when the solution is considered converged is highly subjective, the spike of the overshoot of the SAN signal has been chosen as landmark to create some sort of comparability between the plots. Figure 13a plots the absolute value of the spikes maximum membrane potential over the mesh size, here represented as DOF. Figure 13b plots the time at which the spike reached its maximum over the respective DOF.

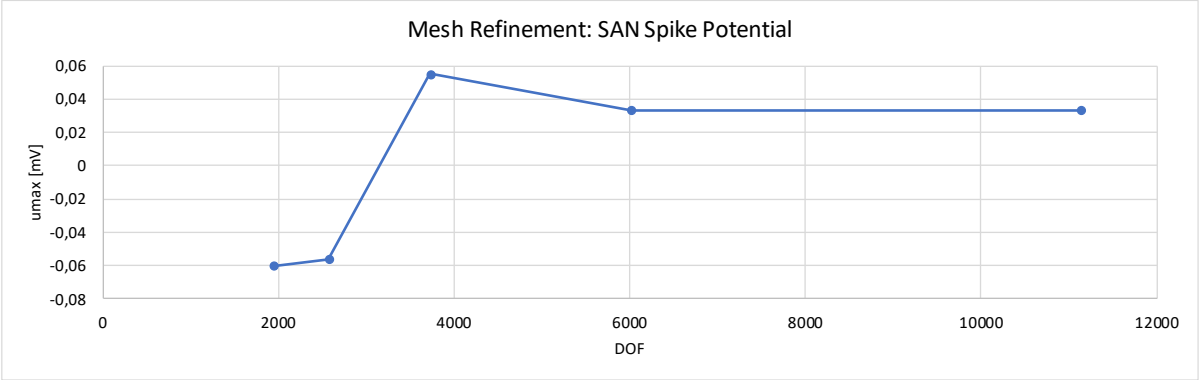

(a): Potential over DOF

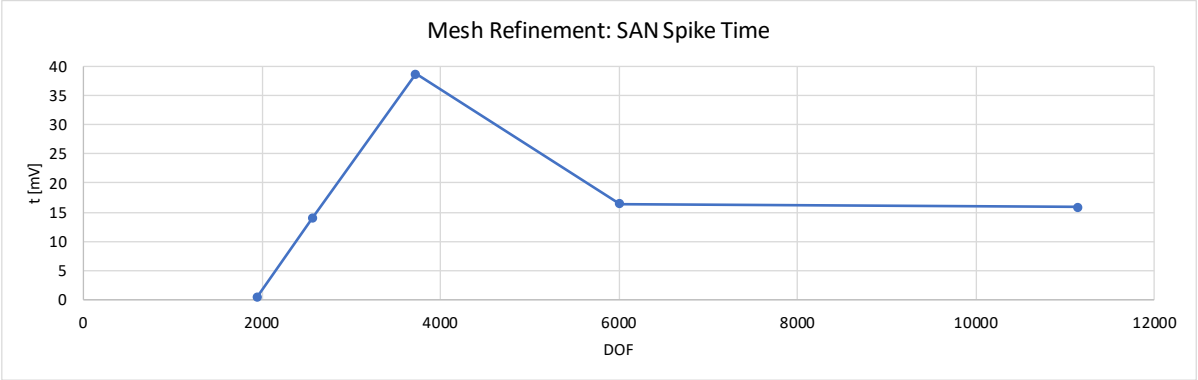

(b): Time over DOF

Figure 13: Mesh Refinement Convergence [own image]

Another feature of the heart mesh is the adaptive meshing around certain areas that are of special interest or detail, such as the region around the SAN. These areas are provided with an even finer mesh than the rest of the heart in order to represent these areas accurately without any loss of detail. A demonstration of the adaptive meshing can be seen in Figure 14

below, which displays the XY-plane of the heart-geometry. The mesh of the SAN and its surrounding area is significantly finer than other areas of the heart.

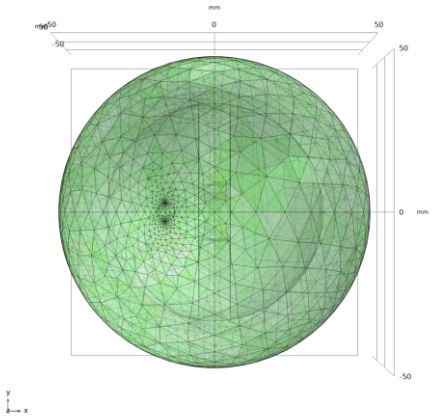

Figure 14: Adaptive Meshing of the Heart-Geometry [own image]

4.1.1. Patient-specific Geometry

The segmentation of the heart in 3D Slicer is a fairly straightforward yet time-consuming task when done manually as the imported DICOM dataset contains the heart and all its surrounding structures which need to be eliminated in order to obtain a clean heart phantom. Figure 15 shows the views of the three anatomical planes with the unedited DICOM data. The heart is visible, yet still surrounded and partially overlapped by adjacent structures such as surrounding bones or tissue. The top right image does not display a 3D-rendered image yet as this would simply be a filled volume cube in this stage.

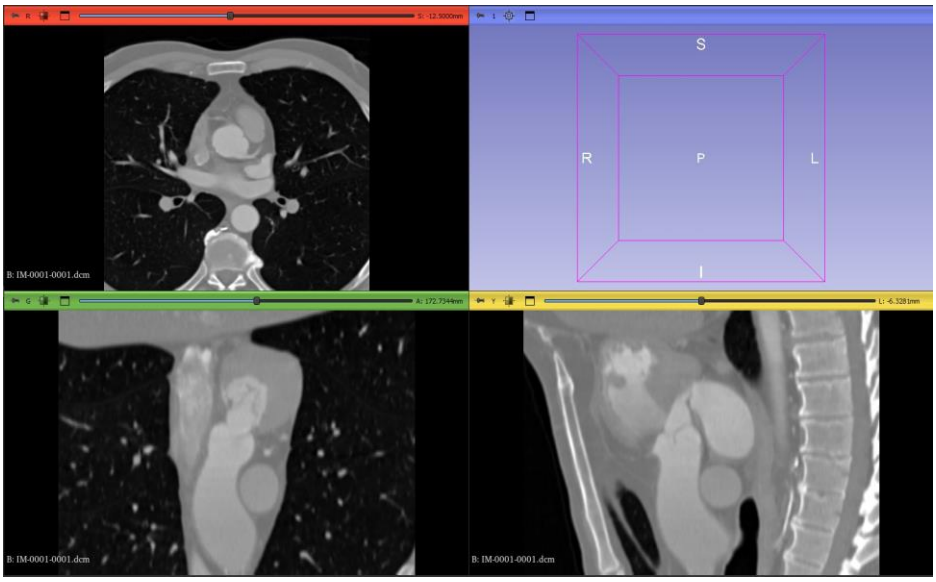

Figure 15: Raw DICOM Dataset imported in 3D Slicer [own image]

The segmentation starts with selecting the region of interest (ROI), first by minimizing it as much as possible around the heart in all three planes. After that, a threshold of an intensity range is selected in a way that as much heart muscle as possible is marked while covering as few other structures as possible at the same time. With the result of these steps as a foundation, the remaining inaccuracies are removed manually until solely heart muscle without holes is included in the selection. The geometries resulting cubical features (due to the shape of the voxels and the tools used) are smoothened by using a gaussian filter. The result can be seen in Figure 16. In this image, the segmentation of the different areas that will be important for calculations later on has already been performed and is made visible by the different colors that appear within the heart. In this case, red represents the volume of the hearts chambers (blood), dark green depicts the working myocardium, light green roughly represents the left and right bundle branches, and the purple spot represents the HIS bundle. The blue layer depicts the isoelectric valve plane between the atria and the ventricles. The top right image depicts the 3D-rendered preview of the model with the already closed vessel openings.

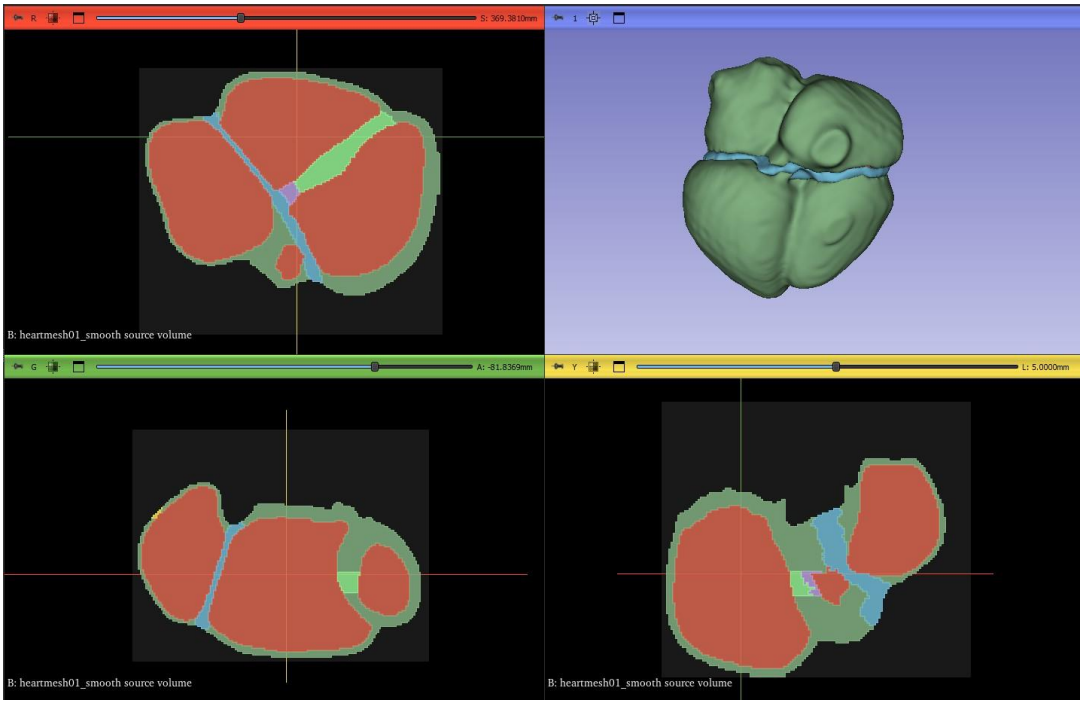

Figure 16: Segmented and smoothed model [own image]

Exported as .obj files, the individual segmentations can be imported into MeshLab where they are meshed automatically upon opening. This auto-generated mesh is extremely fine in order to depict all of the geometries features correctly which is not necessarily beneficial for the purpose of complex calculations later on. Therefore, the mesh is reduced as much as possible while still representing the key aspects of the geometry correctly. In the case of the entire heart

structure with all segments combined, this implied a reduction of vertices, faces and edges by approximately factor 16 (see Table 2).

	Auto-generated Mesh	Refined Mesh	approx. Factor
Vertices	192334	12030	15,988
Edges	577002	36060	16,001
Faces	384668	24040	16,001

Table 2: Simplification of the auto-generated Mesh [own data]

The visible difference between the two meshes is depicted in Figure 17 below. The mesh on the left (a) appears filled because the vertices and edges are so close together that they blur into one surface when viewed in this scale. Details and individual faces are not visible until the image is enlarged. The mesh on the right (b) on the other hand shows distinct faces due to the reduction while still depicting the general shape as well as key characteristics of the original heart model correctly.

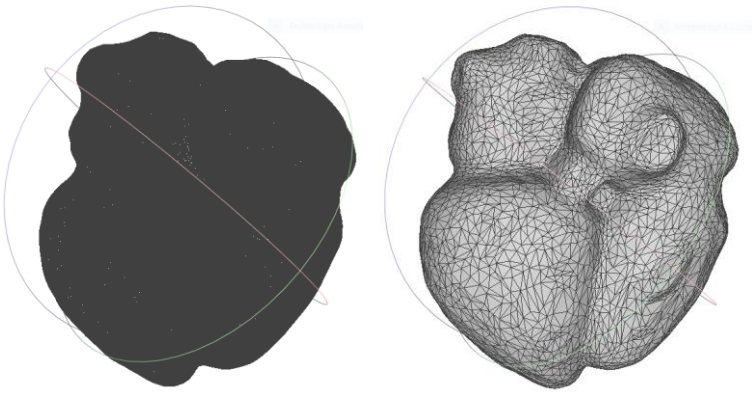

(a) (b)

Figure 17: Mesh simplification [own image]
(a): auto-generated Mesh (~385k faces), (b): refined mesh (~24k faces)

After fixing the mesh by removing holes as well as duplicate edges and vertices, the resulting file can be exported into an STL file which can finally be imported in COMSOL via the mesh section of the model building tree. From there, the mesh can be further refined and adjusted, if necessary. This includes defining the mesh sizes for the individual areas and segments until the mesh corresponds to the expectations and is of sufficient quality. The quality of the mesh is assessed by analyzing the skewness which is a measure for the approximate deviation of the individual mesh elements from the ideal shape (equiangular, in this case equilateral

triangles). The result of this can be seen in Figure 18 where the skewness of each element is indicated by color. As opposed to usual representations of the skewness, COMSOL considers a value of 1 as the ideal value (equiangularity) and values below 0.1 as poor quality. In this case, the mesh appears well-distributed and can be used for further analysis.

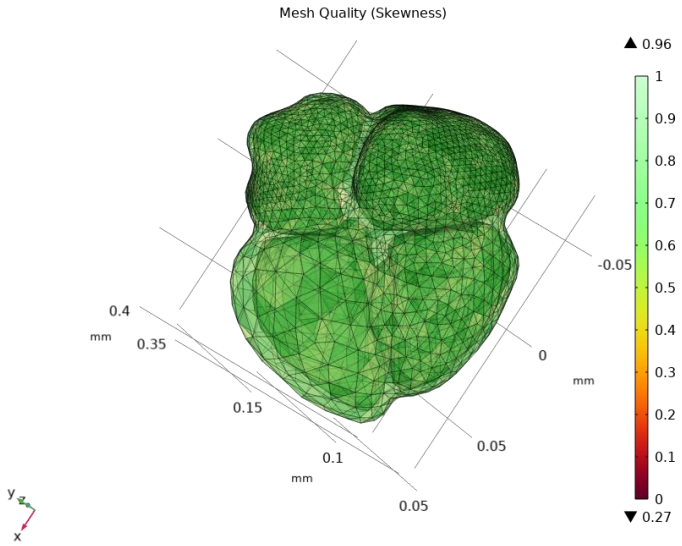

Figure 18: COMSOL Mesh Quality [own image]

As a last step, the different segments of the mesh need to be distributed to the corresponding domains in COMSOL which can simply be done by adding selections in the model building tree and selecting the dedicated segments respectively. Further calculations can then be conducted on the different domains individually.

4.2. Equations

Regarding the implementation of the equations in the simulation, they need to be transformed into a format that is supported by COMSOL. The two main formats for PDEs of this kind are the *coefficient form PDE* and the *general form PDE* which are interchangeable yet differently constructed and can be freely chosen depending on the type of the present PDE. Due to the clarity of the formulation, the coefficient form PDE is chosen in this case whose format looks like the following:

$$e_a \frac{\partial^2 x}{\partial t^2} + d_a \frac{\partial x}{\partial t} + \nabla * (-c\nabla x - \alpha x + \gamma) + \beta * \nabla x + ax = f \qquad \text{Eq. 11}$$

This is the very basic formulation of a generic coefficient form PDE. Further details on this can be found in the COMSOL documentation [35] and will not be elaborated on here as for this case not all of the parameters are needed. When adapting this equation to describe the fast variable *u* by substituting Eq. 9, one is left with the remainder:

$$d_a \frac{\partial u}{\partial t} + \nabla(-c\nabla u) = -ku(u-a)(u-1) - uv \qquad \text{Eq. 12}$$

where c describes the diffusion coefficient which can be set to 0 for both variables in the beginning, but will be introduced later, for more realistic results. For the recovery variable v, the substituted equation looks like this:

$$\frac{\partial v}{\partial t} = (\varepsilon_0 + \frac{\mu_1 v}{u + \mu_2})(-v - ku(u - a - 1)) \qquad \text{Eq. 13}$$

These are the very basic formulations of the AP equations for modelling with finite element software. They still need to undergo specifications and adjustments, depending on the specific model they are used with. One of these adjustments for this simulation is the replacement of Variable d_a in Eq. 12, which denotes the damping coefficient, with the membrane capacitance per unit area C_m. The incorporation of this coefficient is common practice in cardiac modelling, when the cell membrane is considered as a capacitor [41, p. 56]. Another improvement is the introduction of an additional parameter, *b*, which will be used instead of a in Eq. 13 and allows for a more specific adjustment of the behavior of the recovery variable.

Also, because the original AP equations are dimensionless, the scaling is introduced to the equations at this point. The basic principle of the scaling has been adopted from an example application of the COMSOL application gallery [42]. The dimensionless potentials *u* are scaled by the use of the following equations:

$$u_s = \left(\frac{u + 80mV}{100mV}\right)$$

$$\mathrm{t_s} = t_{init} * \left(1 - \mathrm{T}\frac{\mathrm{t_{act}} - \mathrm{t_0}}{\mathrm{t_1} - \mathrm{t_0}}\right). \qquad \text{Eq. 14}$$

with

$$t_{act} = 50ms(1 - \frac{Z}{zL})$$

The first equation scales the dimensionless potential u to millivolts, corresponding to a resting potential of -80 mV and an overshoot of 20 mV in this case. The scaling of the dimensionless time to milliseconds is conducted by regarding a spatial component within the activation time t_{act} in addition to the time parameters. This allows for a distinguished description of the activation time in reference to the Z axis of the heart.
The optimized equations in coefficient form PDE formulation look like the following:

$$C_m \frac{\partial u}{\partial t} + \nabla(-c\nabla u_s) = \frac{100mV}{t_s} - k u_s (u_s - a)(u_s - 1) - u_s v$$

$$\frac{\partial v}{\partial t} + \nabla(-c\nabla v) + a_c v = \frac{1}{t_s} * \left(-\varepsilon_0 k u_s * (u_s - b - 1) - \frac{\mu_1 v^2}{u_s + \mu_2}\right) \quad \text{Eq. 15}$$

with

$$a_c = \frac{1}{t_s} * \left(\varepsilon_0 + \frac{\mu_1}{u_s + \mu_2}\right) * k u_s * (u_s - b - 1)$$

The use of the t_s parameter scales the time component of the equation to seconds, which would otherwise be dimensionless. The introduction of the absorption coefficient a_c in the formulation for variable v has been performed in order to simulate the spatial diffusion of the model more accurately. Its formulation is inspired by the application file [42].
The initial set of parameter values for the model parameters were taken from the original AP model and can be seen in the following Table 3. For the first simulation, all domains were allocated the same set of parameters. Scaling parameters were taken from the application file as well.

Name	Value	Description
Cm	1 F/m²	Cell Membrane Capacitance
c	0 S/m	Conductivity Tensor
a	0.01	Model Parameter
b	0.15	Model Parameter
k	8	Model Parameter
ε0	0.002	Model Parameter
μ1	0.2	Model Parameter
μ2	0.3	Model Parameter
u_{rest}	-85 mV	Resting Potential
u_{act}	70 mV	External Stimulus
t_{init}	12.9 s	Time parameter
T	0.55	Time Parameter
t_0	12 ms	Time Parameter
t_1	75 ms	Time Parameter

Table 3: Initial Parameters [own data, based on [28]]

4.3. Conditions and Coupling

As a first step, initial conditions for the variables need to be set. As the fast variable *u* corresponds to the membrane potential, a variable is introduced as its initial which is defined individually for each domain, depending on the region of the heart and the corresponding physiological resting potential $\mathrm{u_{rest}}$. The initial value for the slow variable *v* is initially set to 0. In addition to the initial values, an external stimulus is needed to excite the system and to initiate the action of the SAN. This can be included in the formulation of the initial values for the fast variable by adding a local condition that defines a specific initial value for a confined space of the geometry, in this case the SAN region. The corresponding formulation looks like the following:

$$u = u_{rest} + u_{act} * (X < -15[mm]) * (X > -12[mm]) * (Y < 5[mm]) * (Y > 5[mm]) * (Z < 47.5[mm]) \quad \text{Eq. 16}$$

While $\mathrm{u_{rest}}$ describes the resting potential of the cells, u_{act} denotes for the external stimulus or activating potential that is used to elicit the excitation. It is multiplied with a set of spatial components, defining a precise region in which the stimulus is effective. Outside of this confined space, the value for the external stimulus is nullified. A similar result can be achieved when adding an additional domain source to the equation node of *u* which assigns a rectangular function to the domain of the SAN. This has the advantage that the duration of the stimulus can be easily defined. However, in this case it produces the same results as the use of Eq. 16.

The next step is to define the required boundary conditions. COMSOL automatically generates a node with the so-called “Zero Flux” boundary condition for each PDE which essentially is a default boundary condition that assigns insulation characteristics to the selected boundaries. As this is unwanted for this simulation scenario because the electrical conduction across the boundary between the heart and the torso is supposed to take place and should not be restricted by this condition, this can be overcome by defining a Neumann boundary condition for the intersecting boundaries between heart and torso. This condition can be set to override the zero flux condition. COMSOL does provide a template for the Neumann boundary condition under the “Flux/Source” node where the equation is already defined and can be specified according to the needs of the model. In this case the formulation is based on the structure of the coefficient form PDE and is employed in the following form:

$$-n * (c\nabla u * \alpha u + \gamma) = g * qu$$

with

$$g = ec.Jx * ec.nx + ec.Jy * ec.ny + ec.Jz * ec.nz \quad \text{Eq. 17}$$

and

$$q = 0.$$

The term *g* denotes the boundary flux and is used to describe the dependent variable in general.

The formulation that is depicted in this equation also acts as part of the coupling between heart and torso as its components are linked to the physics of the torso model (see chapter 3.3). In this formulation the coupling is indicated by the “ec”-prefix which directs to the variable workspace of the electric currents (ec) module. Its variable *J* describes the specific current density while *n* depicts the normal vector at the boundaries for all three spatial components. The second term *q* represents the impedance term and can be neglected in this case as no absorption across the boundary is considered. The Neumann boundary condition for the slow variable *v* deploys the sub-equations $g = 0 \text{ and } q = 0$.
The second part of the coupling is implemented in the *electric currents* module of the torso model. The electric potential at the boundaries between heart and torso needs to be coupled with the heart model in order for the conduction to take place as expected. This is performed by setting the value of the torso’s electric potential v_0 equivalent to the dependent variable *u* (COMSOL notation: *comp1.u*) that depicts the transmembrane potential of the heart model.

4.4. Simulation Settings

As mentioned in chapter 3.4, COMSOL automatically adjusts the study settings when a study node is added to the simulation. Apart from simulation-specific adjustments to the desired time unit and the output time interval, these auto-settings can be adopted for a first impression of the functionality of the model. The most important settings and changes from the default settings of this simulation are shown in the following Table 4.

Attribute	Current value	Default value
Solver Type	Time Dependent	-
Time Unit	ms	s
Shape Function	Lagrange	Lagrange
Element Order	Linear	Quadratic
Output Time Range	(0,5,500)	-
Time Stepping Method	BDF	BDF
Steps taken by Solver	strict	free
Max BDF Order	5	5
Singular Mass Matrix	yes	maybe
Direct Solver	MUMPS	MUMPS
Reuse sparsity pattern	on	off
Segregated Solver	off	on
Iterative Solver	off	on
Fully Coupled Solver	on	off
Linear Solver	Direct	Iterative

Table 4: Simulation Settings Overview [own data]

In addition to these settings, the time stepping scheme will be controlled as this is a likely source of error that can lead to varying results on the same simulation when the output times are adjusted. This phenomenon occurs because the step size of the output times that is entered by the user is not always equivalent to the step size that is used by the time-dependent solver. The solver uses an adaptive time stepping scheme by default which enables it to adjust the step size depending on the rate of change of the solution, making the calculations computationally more efficient. However, this can lead to different results when re-running a simulation with an altered end time. In order to avoid this, the time steps and the initial time step will be fixed to a constant value.

The setup of the solver with these settings leads to a reliable solution with a calculation time of approximately one and a half minutes for a good quality solution with a normal sized mesh.

4.5. Output and Parameter Fitting

4.5.1. Action potentials

The above-mentioned settings and parameters (see Table 3) are mainly adopted from the literature and have not been adjusted specifically to this model and simulation environment yet. The resulting plots of the individual action potentials, divided by region, are displayed in

the following figures. The left one displays the membrane potential u as a function of the time in milliseconds for the designated measuring point in each domain (reference with Figure 8). The one on the right shows the same action potentials but staggered (therefore dimensionless regarding the membrane potential) in order to avoid the overlap of the signals for better visibility.

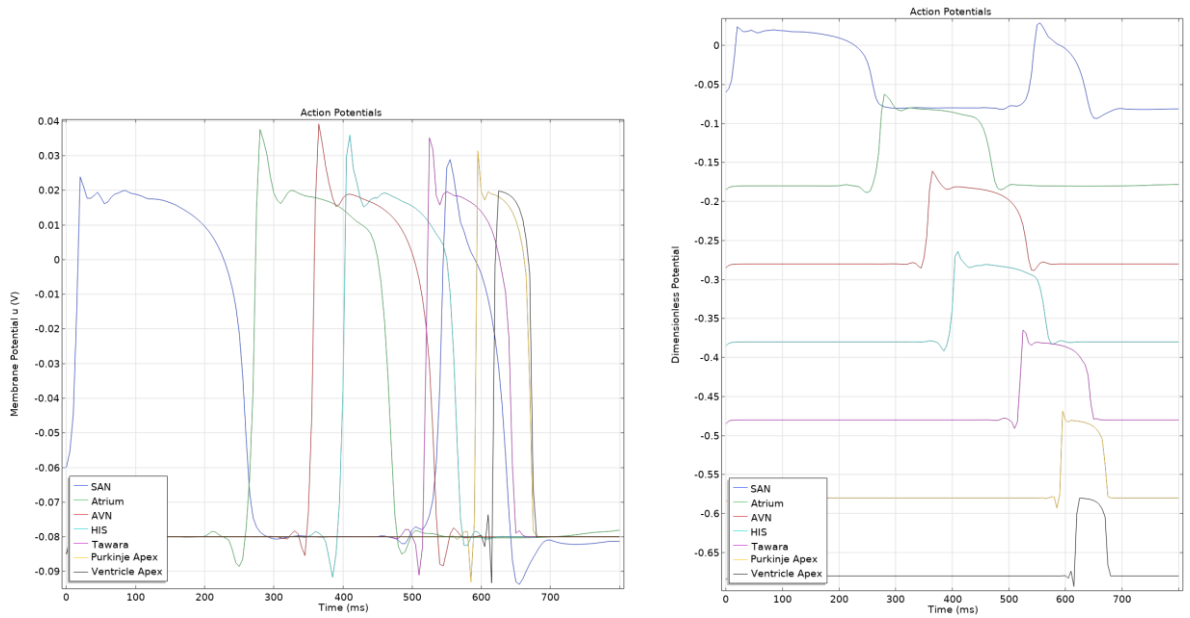

(a) (b)

Figure 19: Output with initial set of parameters [own image]

The shapes of the potentials roughly resemble the expected shapes according to the literature, yet they still need further adjustments with the goal of matching the signals from Figure 19 to the ideal signals from chapter 2.2.2.

The target-performance comparison between them shows some significant differences in the plots, especially regarding the onsets and lengths of the signals. The most noticeable issue is the mismatch of the excitation within the SAN. This includes the frequency of generated action potentials on one hand and the delay in the excitation of subsequent parts on the other. In Figure 19b it can be seen that the SAN generates two action potentials within the 800 ms time frame. This is not only too high of a frequency, but also no physiological behavior as the second excitation falls timely into the excitation of the myocardium which should not occur in physiological conditions due to the presence of the absolute refractory period. Furthermore, the onset of the excitation of the atrium and subsequent parts of the excitation system takes place approximately 300 ms after the excitation of the SAN and needs to be moved forward in order to reduce the gap to the desired delay of approximately 85 ms. Subsequent regions such

as the atrium and the ventricle need to be adjusted regarding their length of excitation as well. Furthermore, the important characteristic of the AVN which is to delay the signal propagation by approximately 100 ms does not show when simulating with the initial parameters and needs to be incorporated.

In order to adjust the parameters, their behavior needs to be examined. This can be done by using COMSOLs parametric sweep function to set a range of values for a parameter and analyze the behavior of the solutions. An example of this can be found in Figure 20. In this case parameter b in the area of the AVN has been chosen for the sweep and is set to a range of (0.1;0.02;0.2). This means that the simulation runs six times consecutively, incrementing the value of the desired parameter according to the defined step size for each run.

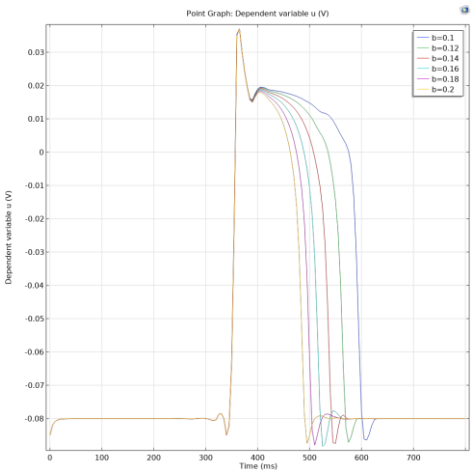

Figure 20: Parametric sweep example [own image]

As depicted in the figure, the result of each simulation is plotted in the same graph and labelled accordingly. This visualization is extremely useful in order to obtain an impression of the assessed parameter's behavior. In this example, the adjustment of parameter b has been performed on the domain of the AVN and it shows that an increase of the parameter value leads to a reduction of signal length and vice versa. Height, overshoot, and general behavior are not affected in this case.

This process is performed for all adjustable parameters until the individual behavior of all of them can be described. Since the model parameters can be adjusted for each domain individually and behave differently depending on the region, they are evaluated for each domain separately. An example for a result of this evaluation, in this case exemplified for the AVN region, is given in the following table.

	Parameter	Initial Value	Domain	Increase ↑	Decrease ↓
Model Parameters	**a**	0.01	AVN	signal compressed	signal expanded
	b	0.15		Plateau reduced	Plateau elongated
	k	8		higher overshoot shift of signal top left	less overshoot shift of signal bottom right
	ε0	0.002		slightly lower plateau shorter signal duration	slightly higher plateau longer signal duration
	μ1	0.2		higher AP frequency, shape distorts easily	lower AP frequency
	μ2	0.3		model is very sensitive to changes, no stable solution when altered	
Time Parameters	**t_{init}**	12.9	AVN	later onset of AP slightly lower frequency	earlier onset of AP slightly higher frequency
	T	0.55		model very sensitive to changes, only small range possible which hardly affects the output	
	t_0	12		delays onset of AP, slightly lower frequency	earlier onset of AP slightly higher frequency
	t_1	75		model very sensitive to changes, only small range possible which hardly affects the output	

Table 5: Parameter behavior AVN [own data]

With a table like this for each of the domains, the individual action potentials can be adjusted experimentally until they match their expected shapes as close as possible. In addition to this, the time scaling parameters were changed from being defined globally for all domains to being listed individually as local parameters in each domain separately. This process leads to the following set of parameters, depending on their locations:

Name	SAN	Atrium	AVN	HIS	Bundle	Purkinje	Ventricle
Cm	1 F/m²	1 F/m²	1 F/m²	1 F/m²	1 F/m²	1 F/m²	1 F/m²
c	0 S/m	0 S/m	0 S/m	0 S/m	0 S/m	0 S/m	0 S/m
a	0.15	0.15	0.18	0.1	0.002	0.15	0.12
b	0.15	0.2	0.16	0.14	0.14	0.13	0.15
k	9,0	8,0	8,0	8,0	9,0	9,0	9,0
ε0	0.00195	0.002	0.002	0.002	0.002	0.002	0.002
μ1	0.195	0.2	0.2	0.2	0.2	0.2	0.2
μ2	0.31	0.3	0.3	0.3	0.3	0.3	0.3
u_{rest}	-60 mV	-85 mV	-85 mV	-85 mV	-85 mV	-85 mV	-85 mV
u_{act}	70 mV	70 mV	70 mV	70 mV	70 mV	70 mV	70 mV
t_{init}	15.9 ms	10.9 ms	10.9 ms	10.9 ms	10.9 ms	10.9 ms	10.9 ms
T	0.55	0.55	0.55	0.55	0.55	0.55	0.55
t_0	15.5 ms	10.0 ms	10.0 ms	10.0 ms	12.0 ms	10.0 ms	10.0 ms
t_1	75.0 ms	75.0 ms	75.0 ms	75.0 ms	75.0 ms	75.0 ms	75.0 ms

Table 6: Adjusted Parameters [own data]

The corresponding output plots are presented in the figure below. Again, diagram (a) on the left shows the original membrane potential scaled to volt, while (b) presents it in a dimensionless and staggered way, for better visibility.

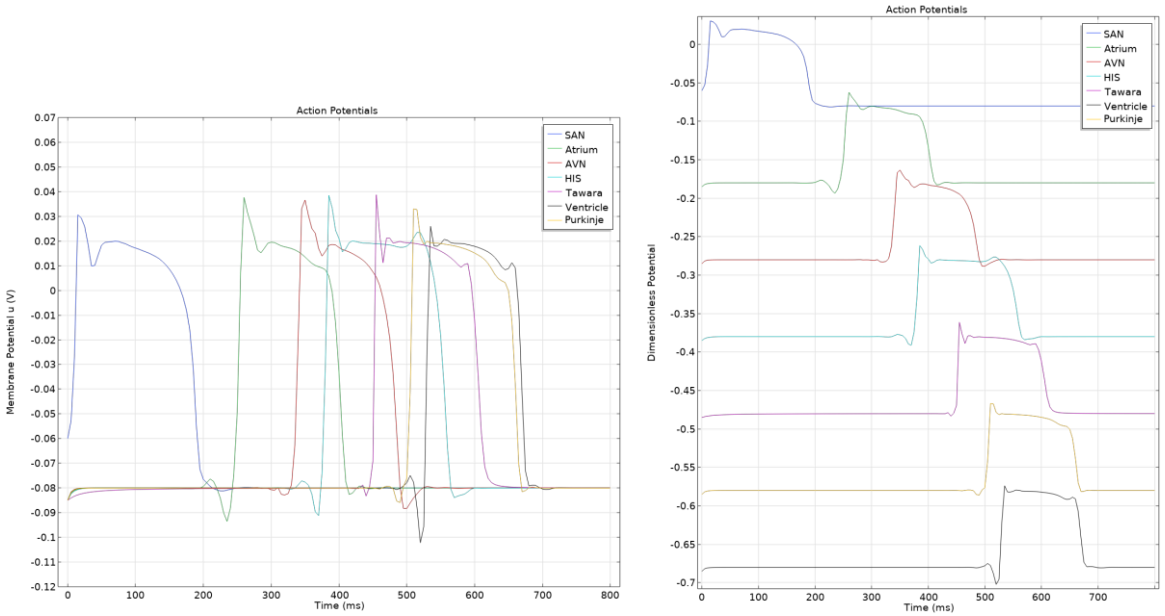

(a) (b)

Figure 21: Action Potentials with adjusted set of parameters [own image]

When evaluating the quality of the results, not only the individual behavior of the action potentials is of importance, but also the spatial behavior of the model, meaning how the excitation propagates across the heart tissue. This can be visualized by generating a two-dimensional surface plot of the heart geometry that depicts the behavior of the signal's propagation across a plane of the heart with the use of a color-coded scale. In this case, the examined variable is the membrane potential u, scaled to volt and displayed at different time points. These plots, corresponding to the simulation with the adjusted parameters, will be shown in the following figure. In all images, the XZ-plane is shown with the position of the slice at the origin of Y (Y=0), cutting through the center of the heart and the SAN. The displayed time points were not chosen linearly, but rather selected based on significant instants of the variable behavior due to the highly time-varying rate of change of the potential.

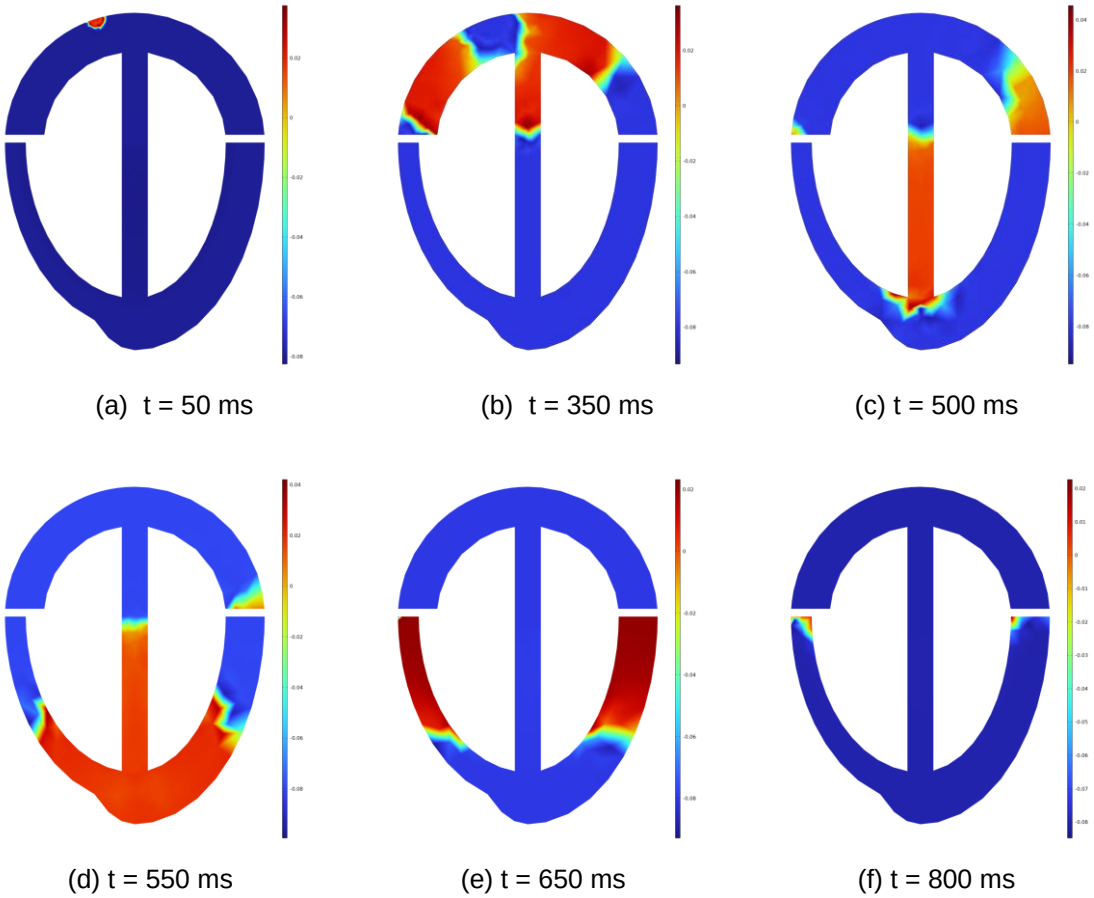

(a) t = 50 ms (b) t = 350 ms (c) t = 500 ms

(d) t = 550 ms (e) t = 650 ms (f) t = 800 ms

Figure 22: 2D Spatial Progression of Excitation [own image]

In order to fully evaluate the spatial propagation, the same principle as described above can be applied to a three-dimensional depiction of the heart-geometry. This projects the membrane potential at a given time on to the three-dimensional heart-geometry, as seen for t=350 ms in the figure below. This allows for a more precise and descriptive visualization of the spatial propagation of the signals as all planes can be viewed at the same time rather than having to calculate each plane individually or as set of three-dimensional slices.

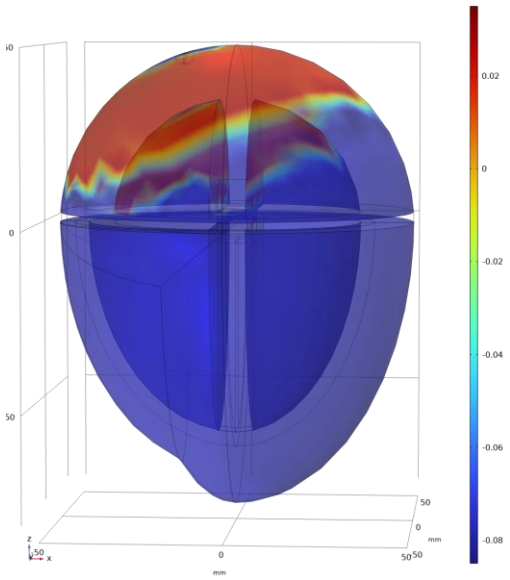

Figure 23: 3D Spatial Progression of Excitation [own image]

4.5.2. Quality and Efficiency

The quality of the solution and therefore the output plot is based on a number of settings that can be adjusted individually or in combination to achieve a solution that is as detailed yet as computationally efficient as possible. These settings need to be evaluated in a way that the best suited compromise between quality and computational load can be found.

Assuming that the geometry and PDEs are set and fixed, the main components that affect the quality and therefore the solution time of the simulation are the mesh of both CAD models and the calculated output times for the simulation. In order to get an impression of how the different settings affect the output, different combinations of the two settings have been evaluated and are displayed in the following Table 7. To provide a sufficient overview of the possible combinations, three states per variable are chosen. In terms of the mesh size this means that a normal, fine, and finer mesh are used in combination with a solver step size of 20, 10, and 5 milliseconds. These combinations produce nine outputs, from lowest (mesh: normal, step size: 20 ms) to highest quality (mesh: finer, step size: 5 ms). For each solution the required computing time is taken together with the visual output in form of the action potential plots. While the numerical results are presented in the following Table 7, the output plots can be found in Appendix B at the end of this paper.

	Settings		Solution	
	Mesh Size Heart	Output Time Step Size [ms]	DOF	Solution Time [s]
I	Normal	20	4232	46
II	Normal	10		48
III	Normal	5		50
IV	Fine	20	6012	64
V	Fine	10		69
VI	Fine	5		71
VII	Finer	20	11142	128
VIII	Finer	10		131
IX	Finer	5		135

Quality - +

Table 7: Solution Quality Overview [own data]

All of these simulations are based on the same physics, the only difference is the change of the aforementioned settings regarding time steps and mesh size. When visualizing these results by plotting the solution time as a function of DOF and step size, the following graphs are obtained.

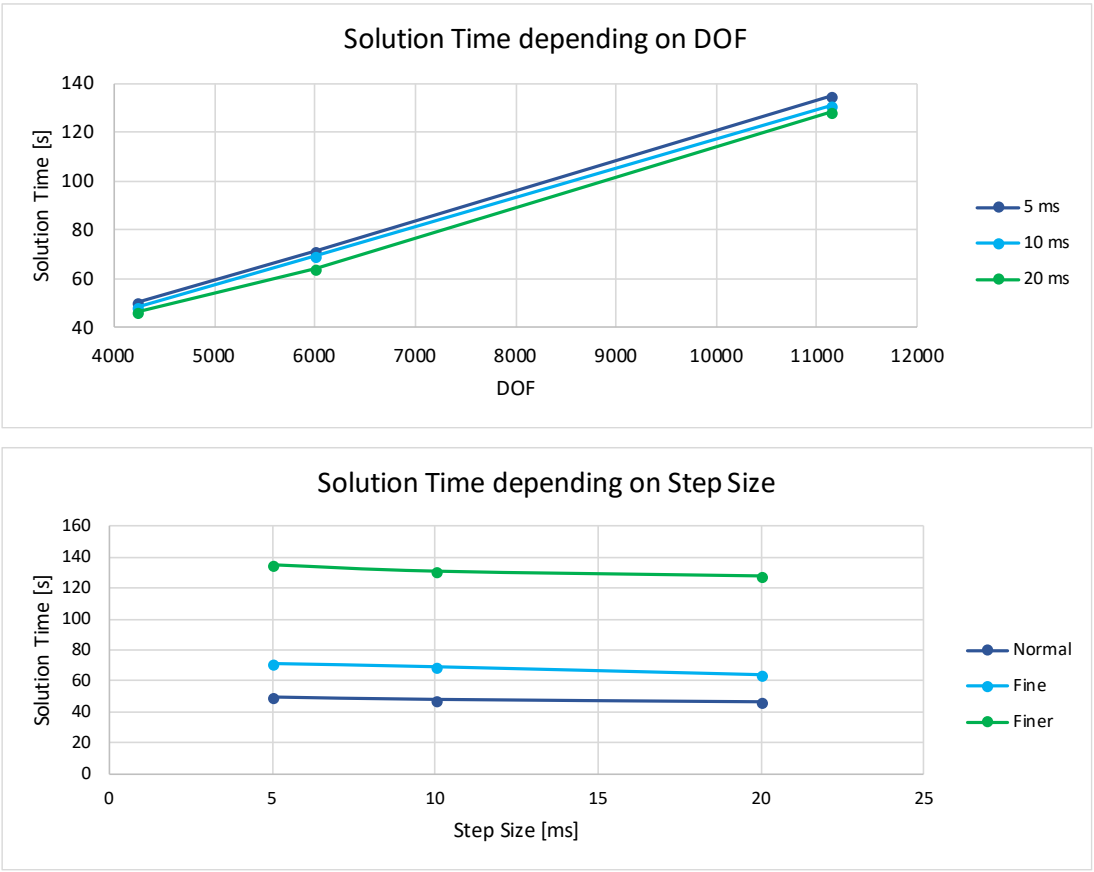

Figure 24: Solution Time evaluation [own image]

The first graph displays the mesh size, here numerically expressed as DOF, on the x-axis. For each of the three sample sizes (5,10, and 20 milliseconds) the required solution times for one simulation are plotted on the y-axis and connected by lines in order to get an impression of the trend.

The same principle has been applied in the second graph with the distinction that here the solution time is plotted against the step size for each of the three mesh sizes.

5. Discussion

5.1. Review of FHN Model

The previous thesis, working on the FHN model approach, provides a solid groundwork for the development of a model that simulates the electrical activity of the heart with the use of FEM software. It presents a conclusive way of using the FHN equations in combination with models of the heart and torso geometry that leads to the generation of action potentials as well as corresponding signals on the torso surface which can be used for the calculation of ECG leads. Although the course of action of the thesis appears conclusive and does not lead to reasonable doubt regarding the procedure, the results are not sufficiently matching their expectations. While most of the generated action potentials do resemble the shape of their corresponding physiological signals to a certain extent, some action potentials were not able to be fitted sufficiently. Mainly the length of action potentials was difficult to adjust which led to deviations in the derived ECG leads.

As the thesis came to the result that the attempt of solving the parameter-adjustment problem with a simple “trial and error” approach based on logic and observations might not be feasible due to the highly non-linear behavior of the parameters and their plurality, this approach has not been further evaluated in the course of this thesis. This decision was backed up by the fact that the general assessment of the model and the settings of the simulation did not lead to the discovery of major flaws which could have been made accountable for the insufficient results. A possible solution to this problem might be the reduction of the model to fewer equations and parameters, likely making the model easier to handle and to maintain due to shorter computing times and less parameter combinations affecting one another. This comes at the expense of risking to compromise the level of detail and flexibility of the model which, in the given context, is not a reasonable approach due to the practical application this model is supposed to fulfill, once finished.
Another approach could be the use of complex parameter fitting algorithms that work with cost functions in order to figure out the best suiting parameters. This concept has briefly been evaluated, but deemed unfit because of the presumably high computational load that comes with the high number of parameter combinations.

Additionally, the explanation of the origin of the FHN model in chapter 2.3.1 suggests that the FHN model is a very basic model that, despite of the modifications and introduction of additional parameters by Dokos et al., is limited in its adaptability to specific requirements and therefore might not have been suitable for the intended purpose in the first place. This is shown by the fact that for some model areas no ideal parameter adjustment was found that

represented the action potential for this area appropriately. This assumption is reinforced by the consideration of other papers that adopt the same approach since they show results with similar inaccuracies in action potential morphologies and therefore related ECG alterations [43].
Therefore, adopting a different approach to describe the ionic currents became apparent and was pursued throughout the course of this thesis.

5.2. Aliev-Panfilov Model

The implementation of the new model based on the Aliev-Panfilov equations was performed on the same geometry as the previous FHN model as it appeared to be a good fit for the purpose of this simulation. Although the results of the attempt to incorporate a patient-specific geometry are promising and indicate that the process of embedding custom geometries into the simulation is feasible, these results have not been tested with the simulation yet. However, the potential for adapting the model to possibly very complex and patient-specific anatomies is interesting and appears suited to be further evaluated once a functioning simulation environment is set up and working sufficiently.
Similarly, the incorporation of the torso model was handled in the course of this thesis. While the theory behind its implementation process was described at the relevant points, the execution was initially omitted. This is due to the fact that at this point of the model building process, the development of a comprehensive and reliable heart model took precedence over the conduction of premature signals in order to generate ECGs.
Therefore, the process of building the heart model was conducted thoroughly and its results will be discussed in the following sections.

Meshing

While the geometry of both heart and torso is adopted from the FHN model without further adjustments, the meshing is optimized by assigning different mesh sizes to the heart and the torso geometry. Furthermore, the individual meshes are, again, scaled in size depending on the region of the model and the desired output quality. This allows a detailed assessment of important and/or quickly changing areas while other less important or slower changing regions are meshed coarser which reduces the computational load without affecting the quality of the solution.
When evaluating the meshes regarding their quality and properties, the histograms in Figure 12 indicate that these meshes are already of a sufficient quality. Nevertheless, a very basic mesh refinement process is performed in order to evaluate the convergence of the solution.

When examining the results of this process (see Figure 13) it can be seen that the solutions seem to converge for mesh size *fine* and *finer*. Although the results for a lower DOF number appear to coincide, it needs to be considered that the value that they converge around (-0.057 mV) is very close to the initial value of the SAN's membrane potential. The agreement of these first two data points therefore needs to be handled with caution. When evaluating the corresponding output plots to the points (see Appendix A), it is obvious that the first two simulations do not generate healthy action potentials. Therefore, the agreement of them can be considered not significant for the purpose of the refinement process and the convergence is assumed to be towards a fine or finer mesh.

Equations

The set of equations that is obtained by reassessing and restructuring the equations of the original AP model facilitates the integration into the COMSOL PDE interface, especially when working with the *coefficient form* PDE formulation. The initial and boundary conditions that were initially stated led to the expected behavior of the system which is why no further changes to them were needed. Regarding the solver settings, several adjustments had to be made in order to adapt the solver to the requirements of the model and the specifications of the geometry. Since multiple varying factors exist that potentially impact the results, settings such as the time stepping scheme, solver tolerances, and temporal and spatial discretization had to be carefully adjusted in order to receive a solution that is as stable yet computationally efficient as possible. The adjustment of the solver settings is a highly complex process due to the complexity of the software and the multitude of possible modifications.

Parameter Fitting

The initial simulations, which assess the behavior of equations and solver on the heart geometry exclusively, already generate action potential shapes that roughly resemble the expected patterns described in the literature. Since these simulations are conducted with the unedited set of parameters that are taken from standard values in the literature, their adjustment to the specific case of this simulation is indicated.

An extensive reevaluation of the parameters with the use of COMSOLs parameter sweeping features leads to the assumption that the parameter behavior can be controlled and anticipated to a certain extent. The experimental adjustment of the parameters shows that the shape of the signals can be altered and modified by changing the model and time parameters of the individual regions. However, the temporal behavior of the signals remains unaffected by this,

implying that the shift of the signals along the x-axis cannot be performed by a simple adjustment of the parameters. A possible solution for this might be the introduction of the exact conduction speeds (according to Table 1) to the individual domains of the model, allowing for the accurate description of the electrical conductivity in each section of the conduction system rather than allocating the same value to the whole heart.
However, the highly non-linearity of the model and the, compared to the FHN model, reduced yet still relatively high number of parameters and possible combinations make it difficult to use full capacity of the possible adjustments without using sophisticated algorithms. The implementation of said algorithms is initially omitted because the main focus at this point is not yet on the precise modulation of the parameters, but rather on the general creation of a stable and adaptable simulation. However, the output generated after a manual yet thorough assessment, followed by adjustment of the parameters, is an improvement on the one based on the unedited parameters, although it does not yet fall within the range of what would be considered a sufficient output for the intended purpose of the model. This is why the application of sophisticated parameter-fitting algorithms should be considered for future development.

Spatial Propagation

When examining the spatial propagation of the signals across the heart tissue (see Figure 22 and Figure 23), the results behave as expected, regarding the propagation across the tissue. Nevertheless, the plots reveal minor discrepancies in the individual action potentials, as mentioned above. One example of this is the too early onset of the HIS-bundle activation which occurs because the physiological delay that is supposed to happen within the AVN is not depicted correctly in the model. As seen in Figure 21, the HIS-bundle is activated while both the atrium and AVN are still depolarized, which is not physiological behavior. This can also be seen in the two-dimensional visualization of the heart when looking at the plot for t=500 ms in Figure 22. It shows that depolarization of the ventricles has already begun with the excitation of the bundle-branches, although the left atrial wall is still depolarized to a significant extent.
However, setting aside discrepancies that originate from deviating action potentials, the overall behavior of the spatial propagation of the signals, as seen in Figure 22 and Figure 23, can be considered good as it aligns with the expected physiological behavior of the excitation-progression across the heart. It also shows that the isolating plane between atria and ventricles works as desired as the excitation passes through the AVN to the HIS-bundle instead of uncoordinatedly across the atrial walls. Considering that this version of the model currently lacks a diffusion coefficient, these results already exceed expectations and hint even further improvement upon the inclusion of a diffusion coefficient.

Furthermore, the three-dimensional plot of the spatial propagation verifies the accuracy of the introduction method of the external stimulus which has been decided on in chapter 4.3. By defining a confined domain in which the activating potential takes effect, the external stimulus can be precisely placed. The success of this method is confirmed by the two- and three-dimensional propagation plots, in which the excitation does start precisely in the location of the SAN.

Simulation Settings

The adjustment of the predefined simulation settings is a critical step in order to obtain a solution that is reliable and computationally efficient at the same time. However, this process is extremely complex and requires a deep understanding of the behavior of the model and the underlying physics of the simulation. Additionally, the successful handling of the software, both technically and in terms of concept, is of great importance in the course of developing a reliable simulation.
While most of the settings can be adjusted by evaluating the physics behind them and consulting COMSOL's extensive documentation, some of them have to be evaluated experimentally, based on the specific needs of this simulation. Some of these settings arise in the course of testing the simulation, for example the discrepancies in the time stepping scheme, as described in chapter 4.4. In this specific case, a minor property of the software led to a huge impact on the solution and inconsistencies in the results. With an assessment of the functionality and behavior of the software, this issue was able to be identified and resolved uncomplicatedly. However, this case emphasizes the importance of adequate knowledge of the desired model and software behavior as well as testing of the simulation. This includes the conduction of several test runs of the simulation with altered parameters, to which the simulation should react robust and remain stable.

Quality and Efficiency

Although the choice of solver settings has the biggest impact on the quality of the solution and the efficiency of the calculations, both can also be influenced by the mesh size and the time stepping scheme that are chosen for the simulation. When regarding the results of the quality and efficiency assessment presented in chapter 4.5.2., the most important observation when reviewing the simulation time graphs is that both of them appear to follow a linear behavior within the evaluated range. In case of the correlation between the solution time and the mesh size, expressed as DOF, a positive linear relationship appears to be present which indicates

that the computational load increases with a constant rate when increasing the mesh size. When evaluating the relationship between the solution time and the step size on the other hand, the correlation is almost constant which implies that the choice of step size hardly influences the required solution time for running a simulation.

When examining the quality of the output plots (Appendix B) on the other hand, the relations are reversed. Although the judgment of the quality of the plots is a rather subjective measure, certain criteria can be expressed that are used in order to contextualize a plot. These criteria include the replicability and accuracy of the output, in this case the conformity of the result with the expected action potential graphs. Another aspect is the consistency and smoothness of the curves. Graphs with unexpected non-smooth behavior or discontinuities are considered of poor quality. Lastly, the resolution of the plots is considered in order to evaluate the sampling rate and the level of detail that is represented by the plot. Due to this substantial number of criteria and the fact that this evaluation is intended to give basic direction rather than an extensive breakdown of the subject, a quantitative analysis of the plots with the use of quantitative metrics and statistics has been omitted at this point.

When taking these points into account while evaluating the output graphs, it quickly becomes obvious that the increase in mesh size does make a difference to the quality of the solution, but only in cases where the solution has not yet converged (meshes of size coarse and normal). On converged solutions (mesh sizes fine and finer), the increase in mesh size does not lead to significant changes in regards of quality. The step size on the other hand appears to have a huge impact on the quality, mainly in terms of resolution because fewer steps lead to the plot of a coarse and non-smooth function which is considered of poor quality as per the criteria defined above.

In conclusion, the quality and the efficiency of the model are related to the mesh and step size of the simulation. The quality strongly depends on the step size while being resistant to changes of the mesh size (within the range of converged solutions). The efficiency on the other hand is hardly affected by changes to the step size whilst being strongly dependent on the mesh size of the model. Considering this correlation, the desired values for both step and mesh size can be freely determined or adjusted, depending on the specific aim of the simulation and the emphasis on the individual aspects.

Computational Load

In conclusion it can be said that this model does have significant advantages over the previously used FHN model in terms of computational performance. While a single simulation of a one-second cardiac cycle takes slightly over twenty minutes on the FHN model, the same

simulation runs on this model in under five minutes, even on a finer mesh than used in the FHN model.
This can be considered a major improvement, not only because the reduction of computing time is a main goal in simulation in general, but also because this has several positive implications on the handling of this simulation. Due to shorter simulation times the throughput of simulations is higher which makes the handling of adjustments, both manual and as sweeps, faster and more efficient. In addition, if the simulation time for a good quality result is already short, there is potential for using a model of even higher quality without having to compromise on an overly extended computing time.

5.3. Limitations

Due to the complexity of the subject and the software, not every aspect of the model-building process could be completed within the given processing time. While the present simulation does generate stable and promising results, there are still some aspects that need to be evaluated and optimized in further studies.

A main issue with the generated action potentials is the inability of the simulation to depict the electrical activity of the atria accurately. Even major adjustments to the parameters did not lead to the reproduction of the desired shapes of the SAN, atrial myocardium, and the AVN. This most likely originates from the fact that the present simulation is based on the AP-model which, in its original formulation, is tailored to describe the electrical activity of the ventricles and not the atria. Given that this is likely the reason for the mismatch between the actual and the expected depiction of the atria in this model, it does not disprove the validity of the whole simulation as the problem can be singled out and be handled discretely. Possible approaches to resolve this issue include the adjustment of the AP-equations for the atria or introducing a completely new set of equations for the atrial region of the model.

Another aspect that is still to be implemented in this simulation is the spatial component of the diffusion across the heart. In the present model, both electrical conduction system and myocardium are treated as media with isotropic characteristics. Because this does not reflect the actual behavior of myocardial tissue, a spatial component needs to be introduced to the simulation to effectuate a physiologically accurate depiction of the diffusion across the tissue. This could be achieved by introducing a suitable diffusion coefficient that takes the fiber orientation of the tissue into account and can be adjusted depending on the needs of the simulation. It appears likely that this would not only improve the overall behavior of the

simulated diffusion across the heart, but also approach the timing issues with the action potentials and their onsets.

Regarding the parameter fitting process, this simulation encounters the same challenges as the previous thesis. Due to the highly non-linear behavior of the parameters, the anticipation of the system's behavior in response to adjusted parameters is extremely difficult when done manually. This leads to the extremely time-consuming task of experimentally fitting the parameters. Although the design of this simulation already simplifies this process compared to the previous thesis by working with a reduced number of adjustable parameters and by a significantly reduced simulation time, the process is still highly ineffective when conducted manually. A possible approach to address this issue is the adjustment of the parameters with the use of parameter-fitting algorithms that can be implemented externally in order to efficiently analyze the model behavior and adjust the parameters accordingly.

5.4. Future Work

Future work on this topic is highly recommended as the results of this paper suggest that addressing aforementioned limitations can lead to a simulation that is capable of meeting the desired requirements as described in chapter 1.2.

One of the main aspects to improve during further research is the incorporation of the diffusion coefficient that controls the spatial propagation of the signals across the heart tissue in the simulation. This is important for simulations that are used in practical applications as it accurately depicts the behavior of physiological heart tissue and can be altered later on when pathophysiological changes are supposed to be simulated. The implementation of this to the presented model is also likely to resolve the issues with the inaccurate timings of the signals as the progression of the excitation across the excitation system can be modelled significantly more precise.

Another aspect that appears interesting to be elaborated on is the incorporation of patient-specific conditions. As seen in this paper, the incorporation of specific heart geometries based on CAT- or MRI-scan files seems possible, nevertheless this process could be made more efficient by automating parts of it. Furthermore, the incorporation of patient-specific torso models appears to be interesting as well, as it enables examining not only the intrinsic properties of the model, but also external influences. One application example for this could be, for instance, the incorporation of anatomical abnormalities of the torso and the investigation of their effect on the derived signals. Also, the impact of common difficulties in the application

of electrodes, such as the presence of an excessive amount of adipose tissue or the decrease in conductibility of the skin when the electrodes are applied on hair, could be evaluated when the torso model is adjustable.

Although these are merely a few possibilities to improve this model, it is evident that the simulation has the potential to be further developed in order to be used in practical applications. Once the heart model meets all required specifications, the coupling with the torso should be conducted in order to evaluate the results of the heart model and their conduction across the torso on body-surface level.

6. Conclusion

To begin with, it can be stated that the initially defined constraint of this topic, to focus on the simulation of the heart model exclusively rather than the complete thorax-model, was reasonable. Due to the complexity of the field of research, the deferment of the coupling with the torso model led to a more profound model building process as it were the case when the torso model would have been handled within the same amount of given processing time. Thereby, a solid foundation of a functioning heart model has been established and presented in this paper, upon which further development of the model can take place.

The decision not to pursue the development of the FHN model approach due to several discrepancies in this model has proven to be reasonable within the course of this thesis, as the implementation of the AP model introduced several advantages to the simulation. These are for example a reduced set of parameters within the employed equations and the significantly reduced computing time, which leads to the calculation of results in approximately one-fifth of the time needed for simulations on the FHN model.

The resulting model, that was developed in this paper, is able to generate practical action potentials that are fairly close to the desired results. While still some flaws are present within the generated results, these mainly affect the timely behavior of the signals, usually depicted by the delayed onsets of individual signals and the missing delay of the excitation within the AVN. These issues are likely to be fixed with the introduction of a diffusion coefficient to the equations and the fiber direction to the heart model, which enables a physiologically correct spatial propagation of the excitation across the heart tissue. While this is only one example for a possible improvement during future work, the model presents a solid basis for several other enhancements that bring it closer to the overarching goal of a complete simulation of the electrophysiology within the heart and thorax. Possible starting points for further development are for one the introduction of and coupling with the torso model, in order to derive ECG leads on the virtual thorax surface and elaborate on the simulation on another level. For another, further interesting enhancements are the incorporation of custom geometries of the heart and torso, adapting the model to particular or patient-specific needs.

Overall, it can be concluded that the model building process that is described in this paper led to the development of a reliable and solid model of the heart’s electrophysiology, which generates sufficient action potentials and represents the spatial propagation across the heart as desired. Although there are still some improvements to be made, this model can be used as a solid foundation for future research to achieve the overarching goal of a complete simulation of the electrophysiological activity within the heart and thorax. Furthermore, this

thesis highlights several additional possibilities for further developments of the model, in order to adapt it to the practical application it is supposed to fulfill upon completion.

Literature

[1] G. A. Roth *et al.,* "Global Burden of Cardiovascular Diseases and Risk Factors, 1990-2019: Update from the GBD 2019 Study," *Journal of the American College of Cardiology*, vol. 76, no. 25, pp. 2982–3021, 2020, doi: 10.1016/j.jacc.2020.11.010.

[2] COMSOL, *COMSOL Multiphysics Software - Understand, Predict, and Optimize.* [Online]. Available: https://www.comsol.com/comsol-multiphysics (accessed: Jan. 30 2024).

[3] A. L. Hodgkin and A. F. Huxley, "A quantitative description of membrane current and its application to conduction and excitation in nerve," *The Journal of physiology*, vol. 117, no. 4, pp. 500–544, 1952, doi: 10.1113/jphysiol.1952.sp004764.

[4] R. Fitzhugh, "Impulses and Physiological States in Theoretical Models of Nerve Membrane," *Biophysical journal*, vol. 1, no. 6, pp. 445–466, 1961, doi: 10.1016/s0006-3495(61)86902-6.

[5] J. M. Rogers and A. D. McCulloch, "A collocation-Galerkin finite element model of cardiac action potential propagation," *IEEE transactions on bio-medical engineering*, vol. 41, no. 8, pp. 743–757, 1994, doi: 10.1109/10.310090.

[6] G. Seemann, F. B. Sachse, M. Karl, D. L. Weiss, V. Heuveline, and O. Dössel, "Framework for Modular, Flexible and Efficient Solving the Cardiac Bidomain Equations Using PETSc," in *Mathematics in Industry, Progress in Industrial Mathematics at ECMI 2008*, A. D. Fitt and J. Norbury, Eds., Berlin, Heidelberg: Springer Berlin Heidelberg, 2010, pp. 363–369.

[7] N. Biasi and A. Tognetti, "Modelling whole heart electrical activity for ischemia and cardiac pacing simulation," *Health Technol.*, vol. 10, no. 4, pp. 837–850, 2020, doi: 10.1007/s12553-020-00417-6.

[8] R. Moss, E. M. Wülfers, S. Schuler, A. Loewe, and G. Seemann, "A Fully-Coupled Electro-Mechanical Whole-Heart Computational Model: Influence of Cardiac Contraction on the ECG," *Frontiers in physiology*, vol. 12, p. 778872, 2021, doi: 10.3389/fphys.2021.778872.

[9] T. Gerach *et al.,* "Electro-Mechanical Whole-Heart Digital Twins: A Fully Coupled Multi-Physics Approach," *Mathematics*, vol. 9, no. 11, p. 1247, 2021, doi: 10.3390/math9111247.

[10] J.-I. Okada *et al.,* "Absence of Rapid Propagation through the Purkinje Network as a Potential Cause of Line Block in the Human Heart with Left Bundle Branch Block," *Frontiers in physiology*, vol. 9, p. 56, 2018, doi: 10.3389/fphys.2018.00056.

[11] R. K. Amanfu and J. J. Saucerman, "Cardiac models in drug discovery and development: a review," *Critical reviews in biomedical engineering*, vol. 39, no. 5, pp. 379–395, 2011, doi: 10.1615/critrevbiomedeng.v39.i5.30.

[12] D. U. J. Keller, D. L. Weiss, O. Dossel, and G. Seemann, "Influence of IKs heterogeneities on the genesis of the T-wave: a computational evaluation," *IEEE transactions on biomedical engineering*, vol. 59, no. 2, pp. 311–322, 2012, doi: 10.1109/TBME.2011.2168397.

[13] M. Buchta, Ed., *Das Physikum: Kompendium zum 1. Abschnitt der Ärztlichen Prüfung,* 2nd ed. München: Elsevier Urban & Fischer, 2010. [Online]. Available: http://institut.elsevierelibrary.de/product/das-physikum3946

[14] Amboss, *Aufbau des Herzens.* [Online]. Available: https://www.amboss.com/de/wissen/Aufbau_des_Herzens/

[15] S. S. Antman, J. E. Marsden, L. Sirovich, J. Keener, and J. Sneyd, *Mathematical Physiology*. New York, NY: Springer New York, 2009.

[16] S. Silbernagl and A. Despopoulos, *Taschenatlas Physiologie,* 8th ed. Stuttgart: Thieme, 2012.

[17] R. Brandes, F. Lang, and R. F. Schmidt, Eds., *Physiologie des Menschen: Mit Pathophysiologie,* 32nd ed. Berlin: Springer, 2020. [Online]. Available: http://www.springer.com/

[18] Amboss, *Herzerregung: Erregungsbildungs- und Erregungsleitungssystem.* [Online]. Available: https://next.amboss.com/de/article/yp0dHS

[19] EKG & ECHO, *Die EKG-Ableitungen: Elektroden, Extremitätenableitungen, Brustwandableitungen, 12-Kanal-EKG.* [Online]. Available: https://ekgecho.de/thema/die-ekg-ableitungen-elektroden-extremitaetenableitungen-brustwandableitungen-12-kanal-ekg/ (accessed: Jan. 30 2024).

[20] A. L. Goldberger, Z. D. Goldberger, and A. Shvilkin, *Goldberger's clinical electrocardiography: A simplified approach*. Philadelphia, PA: Elsevier, 2024.

[21] H. Dathe, D. Krefting, and N. Spicher, "Completing the Cabrera Circle: deriving adaptable leads from ECG limb leads by combining constraints with a correction factor," *Physiological measurement*, vol. 44, no. 10, 2023, doi: 10.1088/1361-6579/acf754.

[22] P. Kligfield *et al.,* "Recommendations for the standardization and interpretation of the electrocardiogram: part I: The electrocardiogram and its technology: a scientific statement from the American Heart Association Electrocardiography and Arrhythmias Committee, Council on Clinical Cardiology; the American College of Cardiology Foundation; and the Heart Rhythm Society: endorsed by the International Society for Computerized Electrocardiology," *Circulation*, vol. 115, no. 10, pp. 1306–1324, 2007, doi: 10.1161/CIRCULATIONAHA.106.180200.

[23] P. Colli-Franzone, L. F. Pavarino, and S. Scacchi, "Mathematical and numerical methods for reaction-diffusion models in electrocardiology," in *MS&A, Modeling of Physiological Flows*, A. Quarteroni et al., Eds., Milano: Springer Milan, 2012, pp. 107–141.

[24] M. Courtemanche, R. J. Ramirez, and S. Nattel, "Ionic mechanisms underlying human atrial action potential properties: insights from a mathematical model," *The American journal of physiology*, vol. 275, no. 1, H301-21, 1998, doi: 10.1152/ajpheart.1998.275.1.H301.

[25] K. H. W. J. ten Tusscher, D. Noble, P. J. Noble, and A. V. Panfilov, "A model for human ventricular tissue," *American journal of physiology. Heart and circulatory physiology*, vol. 286, no. 4, H1573-89, 2004, doi: 10.1152/ajpheart.00794.2003.

[26] J. Nagumo, S. Arimoto, and S. Yoshizawa, "An Active Pulse Transmission Line Simulating Nerve Axon," *Proc. IRE*, vol. 50, no. 10, pp. 2061–2070, 1962, doi: 10.1109/JRPROC.1962.288235.

[27] S. Dokos, S. L. Cloherty, and N. H. Lovell, "Computational model of atrial electrical activation and propagation," *Annual International Conference of the IEEE Engineering in Medicine and Biology Society. IEEE Engineering in Medicine and Biology Society. Annual International Conference*, vol. 2007, pp. 908–911, 2007, doi: 10.1109/IEMBS.2007.4352438.

[28] R. R. Aliev and A. V. Panfilov, "A simple two-variable model of cardiac excitation," *Chaos, Solitons & Fractals*, vol. 7, no. 3, pp. 293–301, 1996, doi: 10.1016/0960-0779(95)00089-5.

[29] R. Jehle, *Physiologie, Pharmakologie, Physik und Messtechnik für Anästhesie und Intensivmedizin*. Berlin, Heidelberg: Springer Berlin Heidelberg, 2023.

[30] E. Vigmond and G. Plank, "Cardiac Modeling," in *Encyclopedia of Biomedical Engineering*, E. Vigmond and G. Plank, Eds.: Elsevier, 2019, pp. 1–20.

[31] Jan Pohlmann, "Entwicklung eines EKG-Simulationsmodells des menschlichen Herzens basierend auf der FitzHugh-Nagumo-Gleichung," Masterthesis, HAW Hamburg, Hamburg, 2022.

[32] F. Arnold Flachskampf, Ed., *Praxis der Echokardiographie,* 2nd ed.: Thieme, 2007.

[33] S. Sovilj, R. Magjarević, A. A. Abed, N. H. Lovell, and S. Dokos, "Simplified 2D Bidomain Model of Whole Heart Electrical Activity and ECG Generation," *Measurement Science Review*, vol. 14, no. 3, pp. 136–143, 2014, doi: 10.2478/msr-2014-0018.

[34] M. Boulakia, S. Cazeau, M. A. Fernández, J.-F. Gerbeau, and N. Zemzemi, "Mathematical modeling of electrocardiograms: a numerical study," *Annals of biomedical engineering*, vol. 38, no. 3, pp. 1071–1097, 2010, doi: 10.1007/s10439-009-9873-0.

[35] COMSOL, *COMSOL Documentation.* [Online]. Available: https://doc.comsol.com/6.2/docserver/#!/com.comsol.help.comsol/helpdesk/helpdesk.html (accessed: Jan. 30 2024).

[36] COMSOL, *What Is Multiphysics?* [Online]. Available: https://www.comsol.de/multiphysics (accessed: Jan. 30 2024).

[37] OsiriX, *DICOM Image sample data sets.* [Online]. Available: https://www.osirix-viewer.com/resources/dicom-image-library/

[38] B. Desjardins and E. A. Kazerooni, "ECG-gated cardiac CT," *AJR. American journal of roentgenology*, vol. 182, no. 4, pp. 993–1010, 2004, doi: 10.2214/ajr.182.4.1820993.

[39] 3D Slicer, *3D Slicer image computing platform.* [Online]. Available: https://www.slicer.org/ (accessed: Jan. 30 2024).

[40] *MeshLab.* [Online]. Available: https://www.meshlab.net/ (accessed: Jan. 30 2024).

[41] J. Keener and J. Sneyd, *Mathematical physiology,* 6th ed. New York: Springer, 1998.

[42] COMSOL, *Biventricular Cardiac Model*. Application ID: 103071. Accessed: Jan. 18 2024. [Online]. Available: https://www.comsol.de/model/biventricular-cardiac-model-103071

[43] S. Sovilj, V. Čeperič, and R. Magjarevič, "3D Cardiac Electrical Activity Model," *Automatika*, vol. 57, no. 2, pp. 540–548, 2016, doi: 10.7305/automatika.2016.10.1620.

Appendix

Appendix A

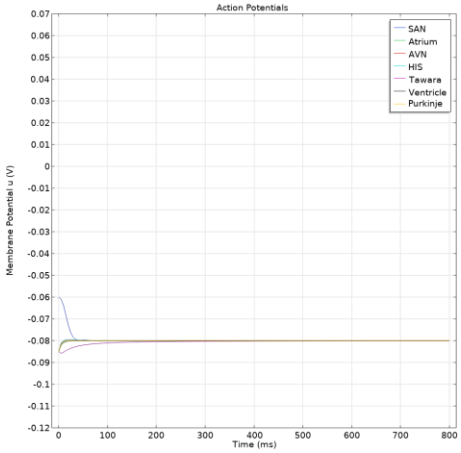

I: Coarser

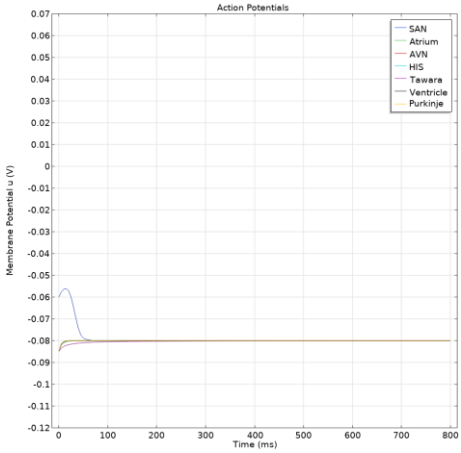

II: Coarse

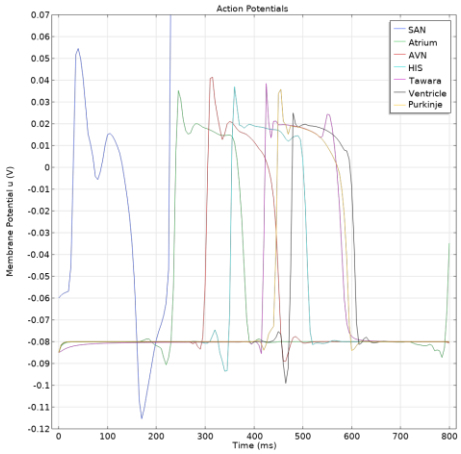

III: Normal

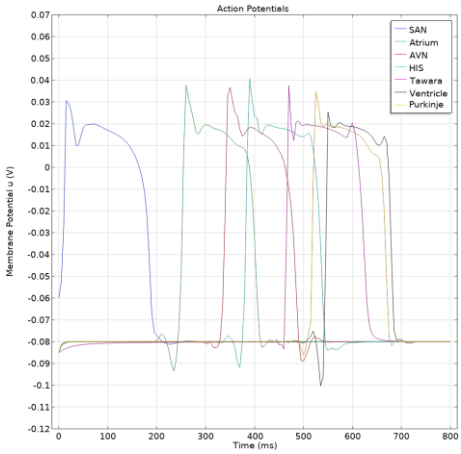

IV: Fine

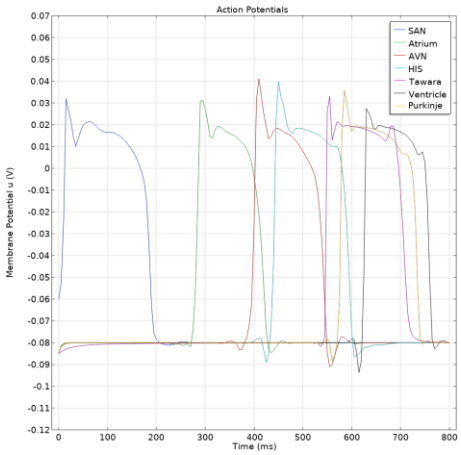

V: Finer

Figure 25: Mesh Refinement Process Output Plots [own image].

Appendix B

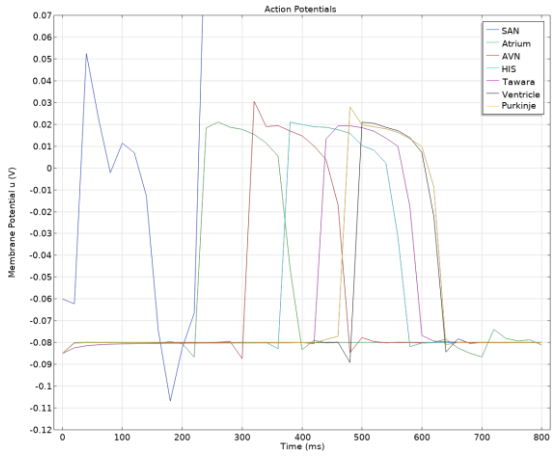

I: mesh normal, step size 5 ms

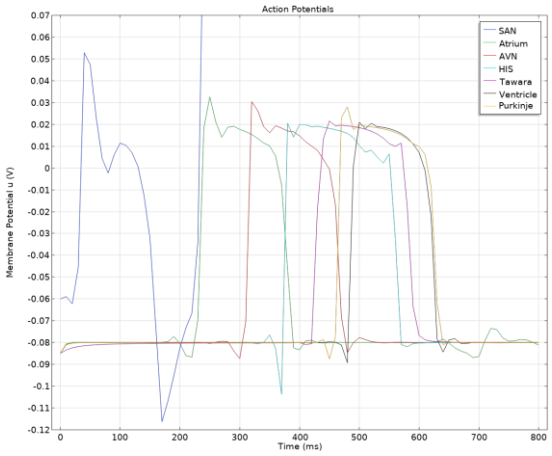

II: mesh normal, step size 10 ms

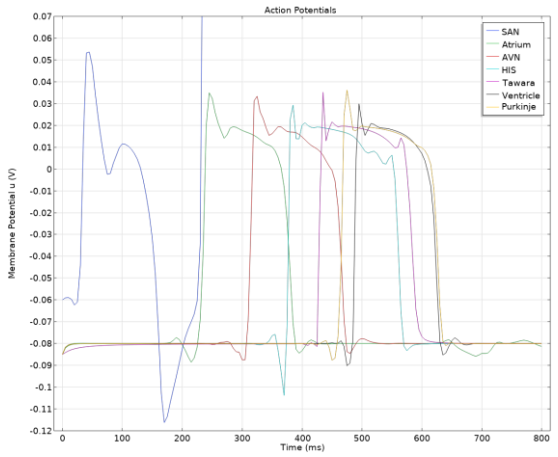

III: mesh normal, step size 20 ms

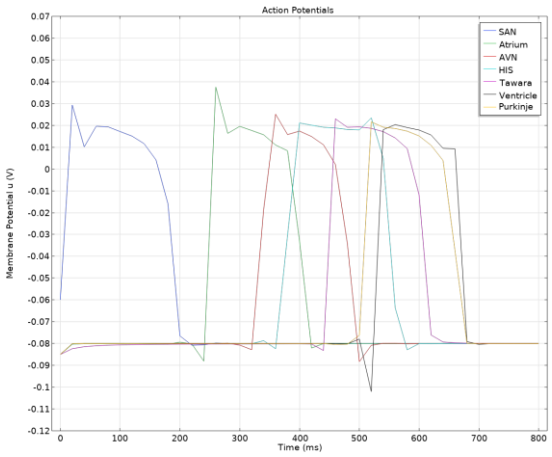

IV: mesh fine, step size 5 ms

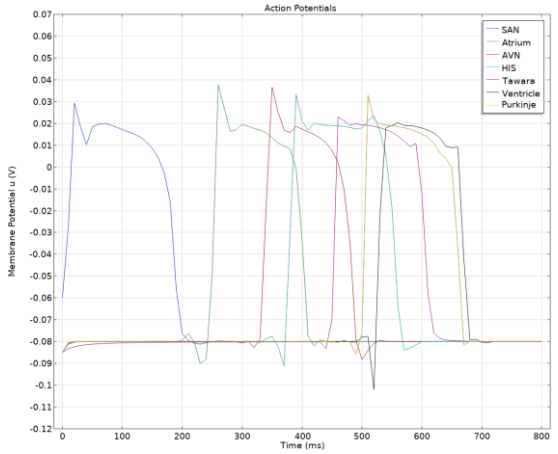

V: mesh fine, step size 10 ms

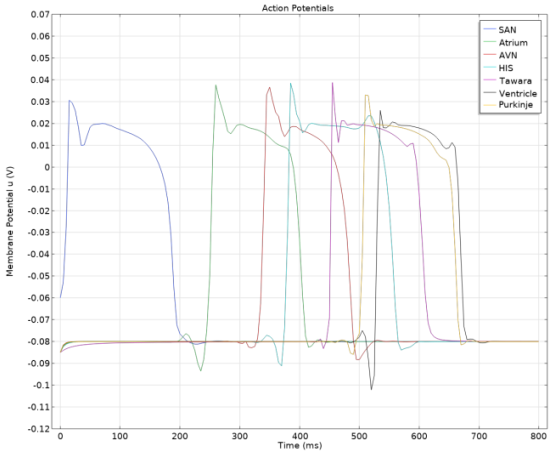

VI: mesh fine, step size 20 ms

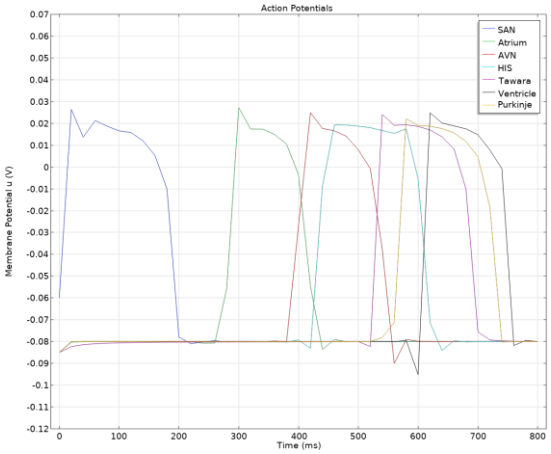

VII: mesh finer, step size 5 ms

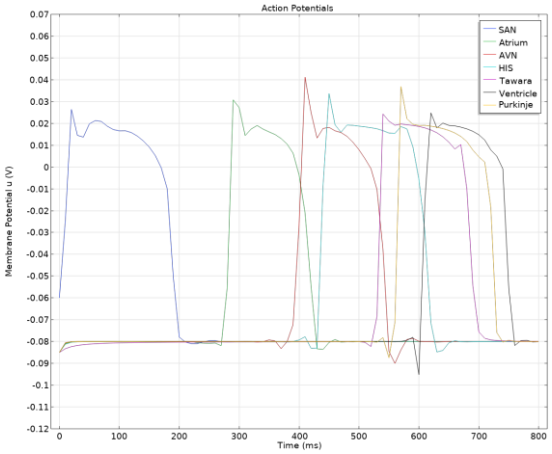

VIII: mesh finer, step size 10 ms

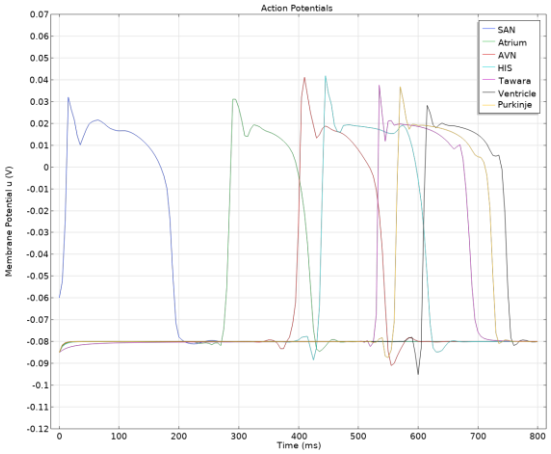

IX: mesh finer, step size 20 ms

Figure 26: Output Plot Quality of Action Potentials [own image].

Declaration of Originality

I hereby confirm that I,

Anna Snaidr

am the sole author of the accompanying thesis with the title:

Simulation of the cardiac electrical activity and derived body ECG using the finite element method

and have written it without contributions from any sources or means other than those cited in the text and acknowledgements. Passages taken verbatim or paraphrased from other works are duly acknowledged by citing the sources.

_____ _____

Place, date Signature